Dear Reviewer #1,

We thank you for the detailed revision of our manuscript. We have considered all your suggestions and we have modified the manuscript accordingly. We believe that the manuscript has been significantly improved in clarity of the text, readability and visualisation of the data in the graphics. Below we provide the answers to the general and detailed comments of the Reviewer.

General comments

It appears that the structure of the manuscript has not been thought through well (e.g. a few singular subsections exist that are not followed by matching subsections) and the manuscript often reads like an extensive lab report. The resulting lengthiness of the manuscript makes it difficult for the reader to grasp the main messages. In addition, the manuscript needs a thorough editorial read (if possible by a native speaker).

A thorough editorial revision of the manuscript has been done. The whole text has been improved for the level of English, the readability and clearness of the independent sections. Many sections have been merged and the stand-alone sub-sections have disappeared. Parts that were too technical and did not need to stay in the manuscript have been moved to the supplement.

The comparison to the in-situ measurements is not very convincing and needs a thorough revision. After studying the manuscript, it is not really clear to the reviewer what new findings have actually been brought up to the table.

The comparison of the retrieved layers by PathfinderTURB with the in-situ measurements at Jungfraujoch is now easier to understand and the correlation between the two datasets is straightforward. Figures 6-9 have been completely re-done.

Point-by-point answer to the Reviewer

The current manuscript is full of acronyms. I suggest to add a table with a summary of all acronyms at the end of the manuscript.

Done.

Page 3: Before describing the retrieval algorithm I would suggest to add a paragraph/ subsection on the instruments being used.

We agree with the Reviewer that a description of the used ceilometer should go before the section describing the PathfinderTURB, we have then moved section 4 after section 2 and right before section 3. Section 4 (now Section 3) has been re-written to improve the readability and avoid all repetitions that occurred in the previous version. The overall section has also been shortened.

Page 5, line 31: Why are different bin heights used for the two different sites? Do the numbers given here relate to the vertical or to the slant path?

We added a phrase to the text to explain the different resolutions used. The different range and time resolutions, with longer integration at KSE, are necessary to compensate the slant path effect and the fact that at KSE the SNR is normally smaller than at PAY due to the smaller concentration of aerosols at these high altitude.

Page 6, line 10: This statement ("... the overlap of the ceilometer is normally sufficiently large ...") implies that there are exceptions. Please clarify.

Yes, each and every ceilometer can have a different receiver-transmitter overlap function, the bi-static ceilometer like the CHM15k can have as large overlap as 0.5 at 350 m, which means that physical measurements of range corrected signal can be performed already at that level.

Page 7, line 7-8: Why are the gradients different for the early morning periods?

The text has been modified and improved for clarity. A full explanation about why we use different thresholds has also been added.

Page 7, Eq. 1 and 2: Please use a more mathematically sound way to describe your formulas (i.e. avoid entire words like 'weights' and use Greek letters instead, also add the specific time and height dependencies).

Done

Page 9: Second sentence is a repetition from page 6.

We have modified the text.

Figure 1: The first and last panel show more or less the same thing and could be combined.

We have preferred to keep the two panels separated in order not to start directly with a panel with many parameters displayed and the weights.

Avoid the sub-panel titles since the date is already given in the caption.

Done

Please define the acronyms in the legend once more in the figure caption. The colour scheme in panel c is not very suitable to detect the overlaying retrieval results.

They all are defined in the current and previous sections.

Page 12, line 9: Here, the full overlap is stated to be at 800 m while on page 6 it is stated to be 350 m. Please clarify.

Here we speak about the full overlap, which for the KSE and PAY ceilometers corresponds to 800 m. Before in the text, the 350 m is just a level situated well above the first overlap point (80 m) and at which physical measurements of range corrected signal can be performed.

Equation 3: It should be S(r; t) to be consistent.

Done

Page 13: Section 4.2.1 is not followed by a section 4.2.2 as one would expect. There are also some repetitions in that section which should be removed (e.g. the information on the tilted angle). Parts of this paragraph are of motivative nature and should be moved to the introduction.

We have moved section 4 after section 2 and right before section 3. Section 4 (now Section 3) has been re-written to improve the readability and avoid all repetitions that occurred in the previous version.

Figure 3: Are both plots really needed here? The lower plot could be moved to the supplement and the key-numbers could be mentioned in the text. The size of the figures is quite large and could be decreased. Please improve the figure caption by avoiding individual acronyms (like 'manualPBL') and by writing full meaningful sentences so that the reader understands the figure without going to the text and finding the acronyms.

We believe that the two plots bring different point of views that allow the reader to understand the different density regions of the comparison between manual and automatic retrieval of the CBLH (top panel), and to have a more detailed and quantitative information about the Gaussian-like shape of the distribution, all statistics and the distribution of the outliers (bottom panel). We have then decided to keep both panels. The caption has been improved for readability.

Page 17, line 18: bR is not defined yet.

The *bR* method is now defined in Section 6.1.

Figure 4: Again, these two panel figures can be reduced to one main figure. The lower panel could be moved to the supplement.

Same as above

Please add uncertainty bars in the scatter plots. The caption is also not consistent with the axis labelling (in the figure MLHbR is shown which is called RS(bR 12H) in the caption).

Done

Page 20: Again, no section 6.1.2 is followed after 6.1.1. Have the authors really carefully thought about the structure of their manuscript?

We removed the sub-section title.

Sect 6.3.3, Table 1 and Figure 7: I have my doubts that these results are really robust and trustworthy. On page 22, line 2-5, the authors state that the results of the LCBLH retrieval for the winter months were not taken into account due to the lack of statistical significance. However, they are now (in terms of the LCBL and CAL reaching JFJ) discussed in detailed and presented in Table 1 and Figure 7.

Figure 7 has been removed (as requested also by the other Reviewer). Figure 6 shows now also the winter daily cycle of TCAL and LCBLH.

If the algorithm can't retrieve the height of the LCBL, how can you be sure that the JFJ is inside the specific layers? This part needs to be thoroughly revised by adding statistical values (like data coverage) to the table. The reader needs to know how trustworthy these values are.

The algorithm PathfinderTURB have no problem retrieving the LCBL when the layer exists and the ceilometer shows it. The winter statistic consist of less data just because the LCBL can rise above the

KSE only rarely during winter. Nevertheless, we have decided to show the winter average daily cycle in Figure 6d and to discuss quantitatively the related statistics. The entire Section 6. has been rewritten accordingly to the new figures and to improve the text clarity.

Figure 7 can be omitted since it is a repetition of Table 1 and nothing new is learned from it.

Figure 7 has been removed.

Section 6.4: The comparison to the in-situ measurements is not very convincing. Why did the authors choose the absorption measurements (MAAP) instead of the scattering measurements (nephelometer)? Most of the signal of the ceilometer comes from particle scattering (backscattering) so I would assume it is more related to the nephelometer measurements.

The author's intention is to study the impact of an aerosols layer on an in-situ measurement that provide a proxy for the presence of the layer itself. In this sense, any extensive aerosol property is an excellent proxy for the presence of an aerosol layer. Moreover, the absorption coefficient is indirectly a measurement of the black carbon concentration, which is a good proxy for CBL air. Incidentally, for most of the studied period, the nephelometer measurements were not available.

Figure 8 is also not convincing at all. All individual seasons show almost no correlation, while the improved annual correlation is therefore only a result of the overall seasonal variations. Besides the fact that the axis ranges in Fig. 8 are poorly chosen, I still don't understand why one would expect a linear relationship. The linear relationships are not at all clearly seen in the figures. Please clarify and revise.

We agree with the Reviewer that the previous Figure 8 was difficult to read and did not bring a straightforward message about the relation between the TCAL/LCBLH and the in-situ measurements. We have decided to change completely the visualization of the sought relation and we have found a clear and robust way to show this relation. The majority of the text has been changed accordingly to the changed figures. The current figures 7, 8 and 9 have now the same layout and are very consistent with each other.

Figure 9: This figure is very difficult to interpret. The differences in the specific seasons are impossible to distinguish. Why would one expect a linear relationship? Maybe plot the seasons separately. The y-axis range should be improved.

As explained above

The conclusion part has to be revised and shortened to the main findings. Currently it is just a repetition of the result section. What have we actually learned?

The Conclusions have been entirely re-written.

In all figures with linear regressions: Please specify which regression type (orthogonal?) has been applied.

No linear regression has been performed anymore in the new plots. So no confusion will arise from it.

For many of the figures it is not clear which averaging time or temporal resolution was used. Also an uncertainty analysis (error bars) are missing which should be added.

All necessary information about data clustering, temporal resolution and uncertainty is now provided for Figures 7, 8 and 9.

Minor comments

Abstract and beginning of section 4: CHM15k is not properly defined.

It is now specified that is a specific type of ceilometer.

Page 9: Add the specific figure number before the panel label (i.e. Fig. 1a).

Done

Page 2, line 31: Define 'TURB' at its first occurrence.

Done

Page 1, line 25: Operating the ceilometer/lidar in a tilted mode is actually not so novel and has been performed at Kleine Scheidegg in previous work (see Zieger et al.(2012), Spatial variation of aerosol optical properties around the highalpine site Jungfraujoch (3580 m a.s.l.), Atmos. Chem. Phys., 1, 7231-7249, doi:10.5194/acp-12-7231-2012).

Thanks to the Reviewer for highlighting the missing reference. Zieger et al have already used a tilted LIDAR at JFJ but only for 9 days back in 2010. What was missing then was the creation of a dataset large enough to create a statistics. The study is now cited and discussed in the introduction.

Page 11, line 24: Remove KSE from the parenthesis.

Done

Page 17, line 33: Mention the specific panel labels.

Done

Page 24, line 3: Two dots

All figures have now a full stop punctuation in the caption (Figure XX.)

Page 24, line 15: I would call them pie charts and not circle charts.

Figure 7 has been removed

Page 25. line 7: I would not use the word 'polluted' here.

"polluted" has been replaced by "aerosol-laden"

Page 27, line 2: Add the missing figure number.

Done

Sect. 6.4 and throughout the text: Define the height of TCAL as TCALH to be consistent with LCBLH.

TCAL is already a height, it is the Top (height) of the CAL.

Figure 9: The superscript in the y-axis label is not properly set.

Figure 9 has been replaced with a new one.

All figures: Please be consistent with the format of your axis labels (i.e. obeying the case sensitivity). If you use acronyms, please define them once more in the figure caption.

Done.

Dear Reviewer #2,

We thank you for the detailed revision of our manuscript. We have considered all your suggestions and we have modified the manuscript accordingly. We have noticed that your review was based on the version of the paper before the technical revision. Nevertheless, the scientific content and the structure of the paper have not changed much after the technical revision. We have then proceeded to the revision of the manuscript based on your comments.

Below we provide the answers to the general and detailed comments of the Reviewer.

General comments

In general the core concepts of the manuscript are presented in a vague and confusing way with many repetitions. This manuscript as currently written will make readers work way too hard to understand the results. It contains too many misspellings and syntax mistakes. In general, could you please try to write shorter sentences (some of them exceed 60 words per sentence!). I suggest, that the manuscript needs a language editing by a native speaker. If the authors could clarify the analysis and structure, it would result in a much improved paper.

A thorough editorial revision of the manuscript has been done. The whole text has been improved for the written English, the readability and clearness of the independent sections. Many sections have been merged in order to clarify the manuscript's structure and all repetitions have been removed. Parts that were too technical and did not need to stay in the manuscript have been moved to the supplement.

Detailed comments

Title p. 1,l.4-5: check order of name and first name.

Done.

Abstract Could you please clarify the structure of the abstract in order to improve readability (e.g. introduction, experimental sites and instrumentation, algorithm, validation, results, conclusion)?

The abstract has been rewritten and shortened. It now reads in a much clearer way.

What is the meaning of TURB in "PathfinderTURB"?

The meaning of the name PathfinderTURB is now provided directly in the introduction.

Manuscript: The extensive use of abbreviations and symbols makes reading the manuscript hard. Could you please reduce the number of abbreviations and symbols used in the ms?

We added a list of acronyms at the end of the manuscript to help finding the meaning of all of them in a same place. Moreover, we tried to limit the use of acronyms where possible throughout the text.

Check space between number and unit throughout the ms.

Done.

Check space between number and unit throughout the ms.

We have moved section 4 after section 2 and right before section 3. Section 4 (now Section 3) has been re-written to improve the readability and avoid all repetitions that occurred in the previous version.

p.3 l.10-13: "The difference between the ML and the CBL is in the 10 term "mixed" (and not "mixing") where the mixed layer indicates a layer in which the profiles 11 of potential temperature and humidity do not vary much in height and the particles and gases 12 are well-mixed, but are not necessarily still mixing." Please delete first part of the sentence. Why do you use italic type for "mixed layer"?.

The sentence has been removed.

p.4, l.1 What do you mean with "atmospheric concentration observations"?

The sentence has been replaced by: "observations of atmospheric compounds at different concentrations".

p.4, l.13 Delete "respectively".

Done

p.5, l.1-8 Maybe this belongs rather to chapter 3?

The paragraph has been shortened and rephrased.

p.6 Suggestion: Describe the Pathfinder algorithm and the new PathfinderTURB algorithm in chapter 3. Please delete the description of the measuring sites. Describe the measuring sites first, so you can refer to this chapter without repeating this information several times in your ms.

Done.

p.7, l.20 "compared with the night"?

The phrase has been replaced by "…the SNR drops below the value 0.6745 already at low altitudes due to the enhanced solar background".

p.14, l.3 "Remote sensing and in-situ observations at Payerne and Kleine Scheidegg". What about the JFJ?

The title of the new Section 3 is now: 3 Description of instruments and sites.

p.14 Please refer only to the measuring devices used in this study.

Done.

p.15, l.9 Please be consistent using "m a.s.l.".

Done.

p. 16 Information about the tilted zenith angle of the ceilometer was given several times

(e.g. p16, 17, 38).

Repetitions have been removed.

p. 16-17 Be consistent when introducing symbols (e.g. p.16, l. 12 vs. l.13, p. 17, l. 12

etc.).

Symbols in the equations and in the text are now consistent with each other.

p.17, l.28 ff. Maybe you put all Methods in a method section and all results in a separate chapter. Try to omit repetitions

Section 5 has been re-written and parts that were too technical and did not bring essential information to the reader have been moved to the Supplement . We tried to remove all repetitions.

p.17, l.32 "We believe" ?.

We have removed it.

p.18, l.2 "Therefore, the PathfinderTURB algorithm".

Done.

p.18, l.10 Please write formulas in a convenient way (a = b+c).

The equation has been removed.

p.18 Please re-write chapter 5.1 "Human expert CBLH retrieval" in a straight way, so that it is easy to understand. Concentrate on the most important facts. Do not use the appendix for repetitions. What is the reason for the division of the experts in the test group and the reference?

Section 5 has been re-written and parts that were too technical and did not bring essential information to the reader have been moved to the Supplement . We tried to remove all repetitions.

p.18,l.9 Remove space between "cases" and full stop.

Done

p. 20,l.10 Change "timeseries" to "time series".

Done.

p.21,l.4 Write "w.r.t" out.

Done

p.22, l.1 What do you mean by "unphysical jumps"?

the sentence has been removed

p.22, chapter 5.2 Could you reduce the number of symbols and abbreviations used in the text. It is way too hard to read the ms.

We added a list of acronyms at the end of the manuscript to help finding the meaning of all of them in a same place. Moreover, we tried to limit the use of acronyms where possible throughout the text.

Be consistent when referring to Figures (Fig. X or Figure X).

Done

p.25,l.14 Change "(Henne at al., 13 2004)This" to "(Henne at al., 13 2004) .This".

Done

p.25-28 seems to be a combination of literature review methods and repetitions.

We have partially re-written and shortened Section 6. Nevertheless, the first part of Section 6 before section 6.1 it's fundamental to explain the dynamics occurring in complex topography.

p.35 "amplitude (max/min)". Delete (max/min)

The whole section does not exist anymore, it has been entirely rewritten.

Fig.1: The quality of the printed graph is not very good. Especially in the third panel it is difficult to differentiate between TCAL and CBH and the background colours.

Figure 1 (now Figure 2) has been edited and the quality improved.

Fig.2: The aerial view is not very meaningful and could be deleted.

Done.

Fig.3 and 4 upper panel: Could you insert the standard deviation or measuring error in

the scatter plots for both methods?

Done.

Fig.3 and 4 upper panel: Could you insert the standard deviation or measuring error in

the scatter plots for both methods?

We added error bars in Figure 4a. The error bars were not possible in Figure 3a, but the RMSE is indicated.

Fig. 6: I don't get the meaning of the left legend. Furthermore, it is not easy to detect the line of the 1h.running median TCAL. Please delete the doubled full stop in the caption (p.31, l.4).

The “iqr” stays for inter-quartile range, this is now clearly stated in the text and the caption. We have enhanced the DPI of the figure and the 1h-running mean line is now more visible. We removed the double full stop.

Fig.8 and 9: Use smaller dots to minimize overlapping dots. Could you please improve readability of the symbols in the legend?

Figures 8 and 9 have been replaced by new figures.

Literature Check order of name and first name (Baars et al. 2008, Balzani et al. 2008), placement of the year (Henne et al. 2010)

Done

PathfinderTURB: an automatic boundary layer algorithm. Development, validation and application to study the impact on in-situ measurements at the Jungfraujoch.

Yann Poltera[1,3], Giovanni Martucci[1], Martine Collaud Coen[1], Maxime Hervo[1], Lukas Emmenegger[2], Stephan Henne[2], Dominik Brunner[2] and Alexander Haefele[1]

[1] Federal Office of Meteorology and Climatology, MeteoSwiss, Payerne, Switzerland

[2] Swiss Federal Laboratories for Materials Science and Technology, Dübendorf, Switzerland

[3] Institute for Atmospheric and Climate Science, ETH Zurich, Zurich, Switzerland

Abstract. ~~Continuous observations of the vertical structure of the planetary boundary layer are invaluable for the validation of atmospheric transport models on the micro and meso scale. Lidar and ceilometer backscatter observations offer a robust technique with growing spatial coverage, but the obtained backscatter profiles need to be carefully translated into boundary layer parameters. Here we~~We present the development of the PathfinderTURB algorithm for the analysis of ceilometer backscatter data and the real-time detection of the vertical structure of the planetary boundary layer. Two ~~typical~~ aerosol layer heights are retrieved by PathfinderTURB: the Convective Boundary Layer (CBL) and the Continuous Aerosol Layer (CAL). PathfinderTURB combines the strengths of gradient- and variance-based methods and addresses the layer attribution problem by adopting a geodesic approach. The algorithm has been applied to one year of data measured by two ~~CHM15k~~ ceilometers of type CHM15k, one operated at the Aerological Observatory of Payerne (491 m, a.s.l.) on the Swiss plateau, and one at the Kleine Scheidegg (2061 m, a.s.l.) in the Swiss Alps. The retrieval of the CBL has been validated at Payerne using two reference methods: (1) manual detections of the CBL height performed by ~~independent~~ human experts using the ceilometer backscatter data ~~of the year 2014~~; (2) values of CBL heights calculated using the Richardson's method from co-located radio sounding data. We found average biases as small as 27 m (53 m) with respect to reference method 1 (method 2). Based on the excellent agreement with the two reference methods, PathfinderTURB has been applied to the ceilometer data at the mountainous site of the Kleine Scheidegg for the period September 2014 till November 2015. At this site, the CHM15k is operated in a ~~novel,~~ tilted configuration at 71° zenith angle to probe the ~~air~~atmosphere next to the Sphinx Observatory (3580 m, a.s.l.) on the Jungfraujoch (JFJ). The analysis of the retrieved layers led to the following results: the CAL reaches the JFJ during 41% of the time in summer and during 21% of the time in winter for a total of 97 days during the two seasons. The season-averaged daily cycles show that the CBL height reaches the JFJ only during short periods (4% of the time~~)~~), but on 20 individual days in summer and never during winter. Especially during summer the CBL and the CAL modify the air sampled in-situ at JFJ, resulting in an unequivocal dependence of the measured absorption coefficient on the height of both layers. This highlights the relevance of retrieving the height of CAL and CBL ~~in mountainous regions~~automatically at the JFJ.

1 Introduction

During convective periods, particles and gases are mixed homogeneously within the convective boundary layer (CBL). The upper limit of the CBL corresponds to the interface between the well-mixed region and the free troposphere (FT) above it. This interface, also called entrainment zone (EZ), is a turbulent transition ~~zone~~of few tens to few hundreds of meters thick characterized by negative buoyancy flux. The ~~description and detection~~study of the EZ and the way the CBL air is mixed through it has drawn particular attention ~~in studies about the CBL dynamics~~ during the last decades. There are various methods to study the CBL and the EZ, based on profiles of temperature, backscatter or turbulence measured either by radio-sounding or by passive and active remote sensing or calculated by numerical models. Amongst the different observational methods, the remote sensing technique ensures the largest amount of profile data. Active remote sensing (acoustic or laser-based) provides the best vertical resolution allowing to resolve the multiple transitions (including the EZ) between different layers in the CBL and the FT. ~~The~~Probably the best-suited instrument ~~used for our~~to study these dynamics at high temporal and vertical resolution is ~~a~~the ceilometer, a low-power, compact and cost-effective version of a research LIDAR. A ceilometer is a laser-based instrument normally ~~single wavelength, and emits linearly polarized laser light~~emitting in the near-infrared spectral band (800-1100 nm), ~~where the signal is~~ highly sensitive to aerosols and cloud droplets. In the early 2000's, the ~~major~~first manufacturers (e.g., Vaisala, Leosphere, MPL, Jenoptik) started producing ceilometers with the capability to store the ~~full~~entire backscatter profile ~~instead of~~in addition to the cloud base ~~only. As a consequence~~height. Rapidly, ceilometers have been ~~rapidly~~ recognized by the ~~national~~ meteorological services and research centres in Europe and worldwide as an efficient and affordable way to study the troposphere using aerosols as tracers (e.g., Münkel, 2007; Flentje et al., 2010; Martucci et al., 2010; Heese et al., 2010; Wiegner and Geiss, 2012; Wiegner et al., 2014). ~~Ceilometers~~Over the last decade, ceilometers have increased significantly in number especially in Europe ~~and the~~, United States ~~especially over the last decade,~~ and Asia , now reaching nearly 1000 units only in Europe ~~alone~~ (http://www.dwd.de/ceilomap). If combined in a single large network, all ceilometers could provide helpful information on the vertical and horizontal distribution of aerosols and on the status of the CBL over a very large geographical domain in near real time.

In order to process automatically a large amount of data over a large and geographically-diverse domain, we need an algorithm capable ~~of retrieving~~to retrieve the vertical structure of the ~~mixed~~boundary layer (~~ML~~BL) during both convective ~~(CBL)~~ and stable ~~(SBL)~~ conditions and over both flat and complex terrain. ~~The term "mixed" (different from "mixing") indicates a layer in which the profiles of potential temperature~~The conditions inside the stable BL (SBL) are generally stratified, and ~~humidity do not vary much in height and~~characterized by strong radiative cooling especially during clear nights. On the ~~particles and gases are well mixed, but are not necessarily still mixing. Whereas, within~~other hand, the CBL ~~there~~ is characterized by an ~~ongoing~~ active mixing ~~normally related~~due to the daytime cycle of thermals updraft and downdraft ~~cycle. Inside the ML (and to some extent also in the FT) several~~ . Several aerosol layers can ~~be formed: an~~ form inside the BL (and into the FT by advection), so the difficulty of discriminating one layer from another is directly proportional to the number of layers. An efficient retrieval method shall ~~then~~ solve the *attribution problem* (layer categorization), i.e. ~~the unambiguous detections of the~~ shall detect unambiguously the different aerosol layers and the EZ. The attribution problem still remains one of the major sources of uncertainty ~~affecting~~related to the ~~ML~~CBL and SBL

Formatted: Font color: Auto

height ~~(MLH)~~ retrieval. In order to ~~respond to these requirements~~address the attribution problem, we have further developed~~, validated and applied~~ the *pathfinder* algorithm originally described by de Bruine et al. (2016~~)~~). We have then validated our own-developed version of pathfinder algorithm and ~~optimized it for the~~applied to real-time ~~detection~~detections of the vertical structure of the ~~CBL. The new~~BL above complex terrain. This improved version of the pathfinder~~,~~ algorithm, is called PathfinderTURB~~, is a gradient~~ (pathfinder algorithm based ~~layer detection algorithm that, in addition to the traditional gradient detection, makes~~ on TURBulence), to highlight the use of ~~the~~ aerosol distribution temporal variability (variance) to detect the ~~MLH. The validated~~BL height. PathfinderTURB has been applied to the data of a ceilometer installed at the Kleine Scheidegg to probe the air ~~that is~~ sampled by the in-situ instrumentation at the high Alpine station Jungfraujoch (JFJ). The JFJ is part of numerous global observation programs like GAW (Global Atmospheric Watch), EMEP (European Monitoring and Evaluation Programme), NDACC (Network for the Detection of Atmospheric Composition Change) and AGAGE (Advanced Global Atmospheric Gases Experiment). Most importantly, in the context of this study, JFJ participates with in-situ observations as a level-1 station in the ICOS project. In contrast to other ICOS sites located over flat terrain, it was decided to install the ceilometer at KSE to characterize the CBL below and above the JFJ. The presence of the aerosols detected by the ceilometer and the frequency at which these reach the JFJ, are directly compared to the optical, chemical and physical in-situ measurements of aerosols and trace gases at the JFJ. Several in-situ instruments are installed at the JFJ and operate continuously since many years to measure aerosols, trace gases and several meteorological parameters (Bukowiecki et al., 2016). Instruments of direct interest to our study are: a condensation particle counter (CPC; TSI Inc., Model 3772), which measures the particle number concentration and two instruments providing aerosol absorption coefficients: a Multi-Angle Absorption Photometer (MAAP) measuring at 637 nm and an aethalometer (AE-31, Magee Scientific) measuring at seven different wavelengths. The fact of measuring remotely with a ceilometer the presence of the ~~ML directly at the JFJ and~~CBL air in real time ~~provides an~~ and close to the JFJ for more than one year is unprecedented ~~possibility~~. A recent study by Zieger et al (2012) has used a scanning LIDAR tilted at 60° Zenith angle for 9 days to probe the air close to the JFJ . Also based on the results of the study by Zieger, we have decided to improve their instrument set-up and to install a ceilometer probing even closer (few meters) to the JFJ and for more than one year. This has allowed to create a statistics of CBL-events and to describe quantitatively the relation between the ~~ML~~CBL dynamics ~~and the aerosols measured in situ at JFJ. An additional motivation comes from the fact that the JFJ contributes with in situ observations of greenhouse gases as a level 1 station to the ICOS (Integrated Carbon Observation System) infrastructure. At level 1 ICOS stations~~ (rising and falling) and the aerosols optical properties at JFJ. The relevance of such measurements becomes also clear in the framework of ICOS, where the detection of the CBL height in ~~their~~the vicinity of a level-1 ICOS stations is ~~required~~a requirement to ~~serve as a validation dataset for~~validate the atmospheric transport models. This is crucial when ~~atmospheric concentration~~ observations ~~should~~of atmospheric compounds at different concentrations must be translated into greenhouse gas fluxes between the atmosphere and the land surface.

~~In Sect. 2, we present an overview of existing algorithms for the retrieval of the MLH from LIDAR backscatter profiles. The novel PathfinderTURB algorithm is then detailed in Sect. 3. In Sect. 4, we describe the configuration of the sites of Payerne (Swiss plateau) and Kleine Scheidegg (Swiss Alps) where ceilometer~~

Formatted: Font: 12 pt, Font color: Black

~~measurements are done. In Sect. 5, we present the validation of PathfinderTURB in Payerne against one year of human expert and co-located radiosonde reference MLH retrievals. In Sect. 6, the retrievals of PathfinderTURB from the recent ceilometer measurements at the Kleine Scheidegg are analysed and compared to the absorption coefficient at 637 nm at JFJ, highlighting the impact of both convective and injection layers on the in situ measurements at the high Alpine station. Finally, conclusions are given in Sect. 7.~~

2 Overview of existing algorithms

Traditionally, the retrieval of the ~~MLH~~BL height from the backscatter profile of a LIDAR can be done using two types of methods: (i) the gradient-based algorithms that track gradients in the vertical distribution of aerosols (gradient of the backscatter profiles), (ii) and the variance-based algorithms that track fluctuations in the temporal distribution of aerosols (variance of the backscatter profiles). Some algorithms combine both techniques, which makes the ~~MLH~~BL height retrieval more robust especially in convective conditions when the ~~ML~~BL dynamics change rapidly.

The gradient-based algorithms retrieve the ~~MLH~~BL height by tracking the well-marked drop in the aerosol concentration that often occurs at the base of (or within) the EZ in convective conditions or at the level of the temperature inversion capping the residual layer (RL), in neutrally-stratified conditions. All vertical negative gradients found starting from the ground are transitions between different aerosol layers and correspond to peaks along the LIDAR backscatter gradient profile. All peaks are labelled as possible candidates of the ~~MLH~~BL height (*layer attribution*) at each time step. The traditional approach using numerical approximations of the first or second derivatives of the LIDAR signal (e.g., Menut et al., 1999), has been improved by using the wavelet covariance transform and the fact that the strong gradient occurring at the top of a layer exists at both small and large scales allowing the wavelet-based methods to reduce the uncertainty when assigning the ~~MLH~~BL height (Davis et al., 2000; Cohn and Angevine, 2000; Brooks, 2003; Baars et al., 2008; Angelini et al., 2009; de Haij et al., 2010; Frey et al., 2010). Alternatively, the Derivative of Gaussian ~~(DOG)~~ wavelet is used in Morille et al. (2007) or the Daubechies wavelets in Engelbart et al. (2008). The Canny edge detection method (Canny, 1986) also helps improving the retrieval of aerosol layers (e.g. STRAT2D: Morille and Haeffelin, 2010). ~~Worth mentioning~~It is also worth to mention the method proposed in Steyn et al. (1999), which consists ~~in~~of fitting an idealized backscatter profile at the transition between the ~~ML~~BL and the FT. In the more recent literature there are examples of different methods combining the LIDAR gradient-based retrievals with temporal height-tracking techniques, for example observational (Martucci et al~~.~~,, 2010a, b), predictive (Tomás et al., 2010) or model-based first guesses (Giuseppe et al., 2012). Pal et al. (2013), proposed a simplified bulk-model combined with surface turbulence measurements and atmospheric variance measurements, to help selecting the ~~MLH~~BL height amongst all candidates. Collaud Coen et al., (2014), used a gradient-based temporal continuity criterion to reduce the problem's degeneration and improve the attribution skill. In the study described by de Bruine et al. (2016) presenting the *pathfinder* algorithm, the gradient field and guiding restrictions are taken as core information to retrieve the ~~MLH~~BL height based on the identification of the most cost-effective path (called a geodesic) along the gradient lines in a graph.

The variance-based algorithms use the temporal fluctuations in the aerosol backscatter as a function of the height z to retrieve the ~~MLH~~BL height. Within the EZ, cleaner, drier free tropospheric air is entrained repeatedly and

mixed-in with the rising aerosol-laden, moister air coming from the ~~ML~~BL. A variance-based algorithm can detect the ~~MLH~~BL height at the level where the backscatter variability reaches a maximum at the base or within the EZ. Variance-based algorithms calculate the temporal variance of the backscatter profile at each range bin, usually over periods shorter than one hour. Similarly to the gradient-based, the variance-based algorithms use peaks in the smoothed variance profile as candidates for the ~~MLH~~BL height (e.g., Hooper and Eloranta, 1986; Piironen and Eloranta, 1995; Menut et al., 1999; Martucci et al., 2007).

Because the transitions between different aerosol layers and between the ~~ML~~BL and the FT are characterized by both a sharp gradient in aerosol concentration and by mixing of air through the interface, the variance- and gradient-based algorithms normally provide similar retrievals of the ~~MLH~~BL height. Still, the gradient-based and the variance-based algorithms have their specific advantages and disadvantages under different atmospheric conditions. Indeed, the depth and structure of the ~~ML~~BL depend on non-linear interactions at different timescales, induced by mechanical and thermodynamic mixing. When retrieving the ~~MLH~~BL height it is then important to include in the algorithm more than one source of information (e.g. gradient, variance, a priori information) in order to account for the largest number of atmospheric conditions and then to minimize the attribution uncertainty. Combining the variance- and gradient-based methods allows to compare the two retrievals at each time step (Lammert and Bösenberg, 2006; Martucci et al., 2010a,b, Toledo et al., 2014). The retrieval method STRAT+ (Pal et al., 2013), based on STRAT2D (Morille and Haeffelin, 2010), uses the Canny edge detection applied to gradient profiles along with the information brought by the variance profiles and by the radiosoundings to detect the main ~~MLH~~BL height and internal boundaries as well as the growth rate.

~~3 PathfinderTURB~~

~~3 In order to retrieve the MLH operationally while minimizing the uncertainty due to the attribution problem and to assure the adaptability of the algorithm to diverse topographical conditions, we have extended the pathfinder algorithm proposed by de Bruine et al. (2016) by adding a variance criterion and the retrieval of the Continuous Aerosol Layer (CAL). The extended version PathfinderTURB has been applied to the ceilometer data at two sites~~Description of instruments and sites

Two ceilometers of type CHM15k-Nimbus (hereafter referred to as only CHM15k) manufactured by Lufft have been deployed for this study at two sites in Switzerland: the Aerological observatory of MeteoSwiss at Payerne (PAY, 491 m a.s.l., 46.799° N, 6.932° E) and the Kleine Scheidegg (KSE, 2061 m~~,~~ a.s.l., 46.547° N, 7.985° E). The CHM15k is a bistatic LIDAR with a Nd:YAG solid-state laser emitting linearly-polarized light at a wavelength of 1064 nm. It has a repetition rate ranging between 5 and 7 kHz, a maximum vertical resolution of 5 m, a maximum range of 15 km, a first overlap point at 80 m and a full overlap reached at 800 m (specific for KSE and PAY ceilometers, Hervo et al., 2016). The standard instrument output is the background-, range- and overlap-corrected, normalized signal S defined at range r and time t as:

$$S(r,t) = \frac{(P(r,t) - B(t))r^2}{C_{CHM}(t)O_{CHM}(r)} \quad (1)$$

Formatted: Font color: Black

Where, B is the background, C_{CHM} is a normalization factor accounting for variations in the sensitivity of the receiver and O_{CHM} is the temporally-constant overlap function provided by the manufacturer. At both sites, PAY and KSE, the overlap function O_{CHM} has been corrected for temperature variations following Hervo et al. (2016).

3.1 Sites description

The PAY site is situated in the centre of the Swiss Plateau between the Jura Mountain range (25 km to the northwest) and the Alpine foothills (20 km to the southeast), as it is shown in the upper panel of Figure 1. The measurement site is characterized by a rural environment leading to biogenic aerosols sources combined with moderate urban emissions characterized by anthropogenic aerosol sources especially related to cars exhaust and house heating. PAY is equipped with numerous meteorological measurements allowing to interpret and to validate the measurements from the CHM15k. The most relevant measurements and instruments in the framework of the presented study are the operational Meteolabor SRS-C34 radiosondes launched twice daily at 00 and 12 UTC (Philipona et al, 2013), and the surface sensors of temperature and humidity. The measurements used for this study at PAY have been collected during the period January-December 2014.

The KSE is located in the Bernese Oberland Alpine region, (Figure 1, bottom panel). KSE is on a saddle point between the mountain peak Lauberhorn (2472 m a.s.l.) to the northwest and the Jungfraujoch (3465 m a.s.l.) to the southeast, and it is a pass between the semi-urban areas of Wengen and Grindelwald. This topographic configuration has a considerable influence on the local wind circulation. Winds at the KSE are mostly blowing along the SW-NE axis (Ketterer et al., 2014), whereas the prevailing wind at JFJ are from NW toward SE. The JFJ itself is located on the ridge formed between the Mönch and the Jungfrau mountains and is 4.5 km to the south-east and 1.5 km higher than KSE. Most of the atmospheric observations at the JFJ are obtained at the Sphinx observatory (3580 m a.s.l.).

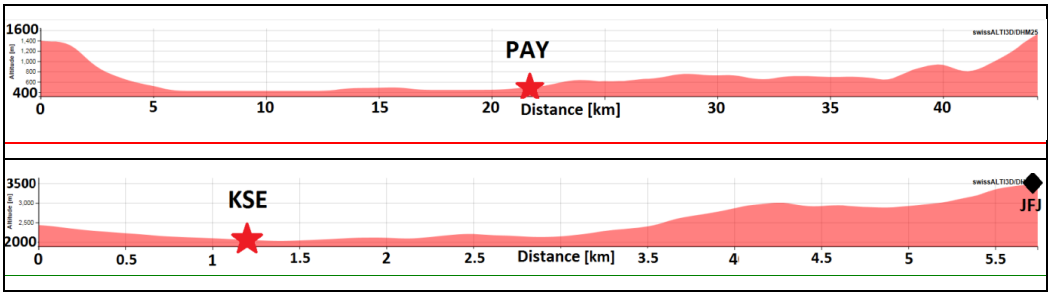

Figure 1. topography of PAY (elevation profile along the 127.2° Azimuth), and KSE (elevation profile along the 151.6° Azimuth) as provided by the federal office of topography (http://www.geo.admin.ch/). The red stars mark the position of the ceilometers at PAY and KSE, the black diamond marks the JFJ position.

Formatted: Heading 2

3.2 Special instrument settings for KSE

The CHM15k ceilometer at KSE was installed in August 2014 on the roof of the maintenance centre of the train station. From September to November 2014 and from March to November 2015, the ceilometer was tilted at 71° zenith angle with the laser beam passing close above (~20 m) the JFJ. From the beginning of November 2014 till

the end of February 2015, the ceilometer was set back to the vertical position (5° zenith angle) to prevent the sun shining directly into the ceilometer's telescope.

The tilted setup of the ceilometer was chosen to observe the injections of CBL air at the level of JFJ and to probe the same air as it is measured by the in-situ instruments at the JFJ. When measuring in slant path the maximum vertical height, R_{max}, depends on the tilt angle and on the instrument's maximum range (15 km for the CHM15k), at 19°elevation angle $R_{\max} = 2.069 + 15\sin(19°) = 6.64$ km a.s.l.. This value of R_{max} corresponds to a level in the atmosphere where aerosols can still be present, this fact represents a problem when the solar background must be removed from the ceilometer signal. The normal procedure of solar background removal consists of subtracting from the ceilometer signal the median value of the signal itself over the last range bins (*far range*). This is only possible when the *far range* is not contaminated by aerosols or clouds. In order to overcome this problem a new technique of background removal depending on $VAR(S)$ has been developed and applied to each profile. $VAR(S)$ is calculated within spatial windows of 120 m to 1600 m width (in steps of 120 m) and computed for all range bins between 390 m and 14970 m. The background corresponds to the median value of S over an optimal window. The optimal window's position is the one minimizing the average of its $VAR(S)$ values. The optimal window's width is the one corresponding to the 75th percentile of the $VAR(S)$ values at the optimal window's position. If it is true that the background correction needs more attention when measuring at tilted angle, a clear advantage related to in the slant path is that once the ceilometer's beam reach the JFJ at 4.8 km the received signal is already in the full overlap region.

4 PathfinderTURB

PathfinderTURB adds a variance criterion to the original pathfinder scheme to retrieve the Continuous Aerosol Layer (CAL) and the CBL. The uncertainty related to the retrieval of the CBL and CAL is minimized by using the geodesic approach, which also allows a better adaptability of the algorithm to complex topography normally characterized by multiple aerosol layers. In the framework of de Bruine's work, the pathfinder technique was applied to the measurements ~~at~~of the tall-tower ~~site of~~at the Cabauw site in the Netherlands and successfully validated by radiosonde (RS) data. Compared to other algorithms, ~~the advantage of the~~ pathfinder (and ~~of~~ PathfinderTURB) ~~is in the ability to~~can solve directly the attribution problem by ~~constructing~~building a ~~timeseries~~time series of ~~boundary layer's~~CBL (and CAL) heights ~~based on~~using the geodesic approach between ~~consecutive~~adjacent points ~~minimizing a well constructed~~ (minimization of the cost function~~. Compared to *pathfinder*,~~). PathfinderTURB ~~uses the variance based retrieval method in conjunction with the gradient based to calculate the geodesic and to retrieve the boundary layer's height while solving the attribution problem. The layers retrieved by PathfinderTURB are the CBL, retrieved only during daytime,~~has been applied to the ceilometer data at PAY and ~~the CAL (defined in the next section).~~KSE.

~~3.~~4.1 Calculation of the Top of Continuous Aerosol Layer ~~(TCAL)~~

The CAL is defined as the uninterrupted aerosol region along the backscatter profile starting from the ground and reaching the first discontinuity in the aerosol distribution. The top of the CAL (TCAL) is ~~then~~ defined as the

Formatted: Font color: Black

Formatted: Font: Not Italic

Formatted: Font: Not Italic

Formatted: Font: Not Italic

height of the retrieved discontinuity. ~~In terms of LIDAR backscatter profile, the CAL is the part of the profile that is not interrupted by a Rayleigh backscatter layer (purely molecular).~~ The criteria to define the CAL are the following (see also Supplement S4):

1. ~~The~~*Signal condition*: the total (aerosol plus molecular) attenuated backscatter is larger than a threshold *Th* that depends on the purely molecular backscatter profile at the ceilometer's wavelength.
2. ~~The~~*SNR condition*: the signal-to-noise ratio (SNR) is larger than 0.6745.

~~Based only on condition 1 (*signal condition*), the TCAL is found at the height where the signal is larger than *Th* and, over~~Over flat homogeneous terrain, ~~it~~the TCAL usually corresponds to the top of the RL during night and to the height of the CBL during day. In complex and mountainous terrain, during daytime, the TCAL corresponds rather to the top of the so-called *injection layer*. The injection layer ~~was~~has been defined by Henne et al. (2004) as the layer formed by injections of CBL air ~~to~~at higher levels. The injections are engendered by thermally-driven converging slope winds along the topography ~~that is~~ reaching higher than the average in-valley CBL top. In contrast to the CBL, the injection layer is only sporadically mixed and indirectly connected to the surface. ~~Condition 2 (~~The *SNR condition*~~),~~ imposes that the SNR is larger than the ~~Gaussian-distributed~~ 1-sigma value of the signal noise. In other words, because the background signal (dark current plus stray light) is range-independent and is considered to be Gaussian-distributed, the backscatter signal is considered noisy when it lies within the 50%-confidence interval of the background signal. ~~The statistics of the background signal distribution are~~The noise is calculated in the far-range of the total signal. If the *SNR condition* is included, the retrieved TCAL can be shallower compared to when only the *signal condition* is taken into account. That happens especially during daytime when the SNR drops below the value 0.6745 already at ~~lower altitude compared with~~low altitudes due to the ~~night.~~enhanced solar background. In cases like this we cannot speak anymore of TCAL, but rather of maximum detected range. ~~Depending on the sky conditions, if~~When clouds are present, also the height of the first cloud layer detected by the ceilometer combined with the heights obtained by the *SNR condition* and *signal* ~~conditions~~*condition* determine the TCAL.

Formatted: Font: Italic

~~3.2 Selection criteria and the main assumption of PathfinderTURB~~

4.2 Calculation of the Convective Boundary Layer Height

For a given day, the temporal evolution of the ceilometer signal is a matrix in time and space ~~where each~~. Each column of the matrix represents a profile at time *t* and constant range resolution. The noise level is calculated from the photon counting signal using the method described by Morille et al. (2007). The signal is ~~binned~~ smoothed in space and time at ~~a resolution~~resolutions of ~~(~~30 m~~,~~ and 1 ~~min)~~minute at PAY and ~~(~~, to compensate the reduced range due to the slant path, of 45 m~~, 2min)~~ and 2 minutes at KSE, ~~then smoothed in time and range.~~respectively. We provide here a description of the main selection criteria and the main assumptions on which the CBL retrieval by PathfinderTURB is based. Further details ~~of~~about the algorithm, including the calculation of the atmospheric variability (signal variance ~~at the micro scale~~) and of the turbulence-enhanced zones, and the mathematical steps leading to the expressions of the measured variables ~~is~~are given in the Supplement (S1, S2).

~~3.2.1~~4.2.1 Lower altitude limit

Close to the ground, for most of the industrial bistatic ~~ceilometer~~ceilometers, the overlap between the transmitter and receiver is ~~missing or~~ close to zero. In this region, called blind region, the returned signal is ~~absent or~~ extremely weak, dominated by the noise and it oscillates around zero. It is thus not possible to retrieve the CBL height (CBLH) in this region (low clouds or fog detections are however possible). Above this region, the overlap increases until becoming ~~full~~complete and the noise component becomes negligible compared to the signal at least within ~~the CBL~~aerosol layers. A positive gradient is then expected at the transition between the blind region and the region above. We thus define the lower altitude limit, *minH*, as the first range where ~~there is a~~the transition from a zero to a positive gradient occurs and we impose *minH* not to be higher than 350 m (where the overlap of the ceilometer is normally sufficiently large to allow physical measurements).

During the morning and until the end of the afternoon, ~~we expect~~ the CBLH ~~to lie at least above~~exceeds the ~~first region from the ground where turbulence is observed. Therefore, an~~height *minH* due to its convective growth. An additional ~~inferior~~lower limit for the altitude is $minH_{TURB}$ ~~is set~~, which ~~delimits~~marks the ~~first appearance~~onset of turbulence~~, and that is derived from the calculation~~ starting from the ground. Turbulence is calculated based on the temporal variation of the LIDAR signal for each *z*-level due to the atmospheric variability. The lower altitude limit *minH* is replaced by $minH_{TURB}$ whenever the latter is higher than the former. The selected minimum limit is called *liminf* in Figure 1.

Formatted: English (U.K.)

~~3.2.2~~4.2.2 Upper altitude limit

Different criteria are defined to calculate the upper altitude limit, *maxH*. These criteria are based on the a priori knowledge of the climatological ~~values of the~~ CBLH value at a specific site (*climatological limit*) and on the ~~retrievals of different~~retrieval of other aerosol and cloud layers ~~made before the~~that contribute to determine the actual CBLH ~~retrieval~~. These ~~retrievals~~layers are: the TCAL ~~(which includes the SNR limitation),~~ the cloud base height (*cloud limit*), and the mixing discontinuities (strong negative and positive gradients). The minimum altitude amongst the three limits determines the upper altitude limit, *limphys*, shown in Figure 1.

Formatted: Font: Not Italic

Climatological limit

A climatological limit can be set based on visually-inspected ceilometer data from previous years and on model-simulated CBLH. The climatological limit depends on the site, and ~~needs as input~~ consists of a maximal ~~constant~~ CBLH value ~~for~~kept constant during the early morning, a maximal mean growth rate until the onset of the afternoon~~,~~ decay and a maximal ~~mean growth rate between the two periods. Hereafter,~~ CBLH value kept constant after the convective growth . For the PAY site, the period called "early morning~~ period is considered as the period starting~~" starts at sunrise and ~~ending~~ends 2.5 hours (~~PAY, 3h~~3 hours at KSE) after sunrise. This period ~~reflects a coarse estimate of the delay in~~to the time-shifted onset convective plume ~~formation~~ and is ~~considered~~assumed constant through the year. The afternoon period is considered to end at sunset. For our study we used the limits 1500 m a.s.l, 3000 m a.s.l and 1 km/h for PAY and 3069 m a.s.l., 4069 m a.s.l and 1 km/h for KSE for morning maximum CBLH, afternoon maximum CBLH and maximum mean growth rate, respectively.

Cloud limit

Two types of clouds are considered: CBL clouds and non-CBL clouds. All cloud information (number of cloud layers, cloud ~~bases~~base, cloud ~~depths~~depth) are provided by the ceilometer's standard outputs. A CBL cloud is defined as a cloud detected by the ceilometer in the first (lower) layer, whose vertical depth is less than 500 m and whose top (cloud base + depth) is lower than the site-specific climatological CBLH limit set ~~before~~beforehand. This criterion is purely mathematical as the cloud depth provided by the ceilometer just gives the depth of the not-totally attenuated part of the signal and not the real depth.

Strong negative and positive gradients

Strong positive or negative gradients indicate ~~mixing~~ discontinuities in the vertical aerosol distribution and can then ~~be taken as limits of~~ correspond to the CBLH. ~~The sensitivity to~~ Strong positive gradients ~~is higher than to negative gradients, because these~~ indicate normally a change ~~of layer~~ from ~~the~~an FT region to an aerosol layer or a cloud base~~.~~ or from a CBL region to a cloud base. Strong negative gradients correspond to a signal drop between two adjacent gradient points of 25% (only 15% during the early morning period due to the still present RL above the forming CBL), whereas strong positive gradients correspond to a signal gain between two adjacent gradient points of 15% (only 5% during the early morning period due to the optically thin fog layer often lifted above the forming CBL).

~~3.2.3~~4.2.3 Growth rate ~~induced refinement~~

~~The~~Once the validity of the limits is ~~checked~~accepted (e.g. the lower limit ~~cannot be higher than~~not exceeding the upper limit~~). Then~~), the limits are recalculated ~~backwards~~back in time ~~(i.e.~~ from 23:59 to 00:00~~), taking into account~~, imposing a growth rate ~~limited to~~of ±0.625m/s between two time steps (i.e. ~~only jumps~~Δz < 37.5 m at PAY and < 75 m at KSE ~~in altitude are allowed between two time steps~~). This growth rate is larger than the climatological growth rate of 1 km/h, because it allows larger jumps over shorter time steps in order to account for the convective dynamics, e.g. updraft and downdraft cycle.

~~3.2.4~~4.2.4 Weights

At each time step ~~*t* and at each altitude *z*~~, a weight ~~is defined as~~function Ω defines the "cost" of ~~passing by (*t*, *z*), i.e. based on the values of the gradient and the variance at (*t*, *z*), the weight says how much it costs to choose~~attributing the CBLH at ~~that~~the altitude ~~and time~~*z* . The weights are calculated by PathfinderTURB as the product of the gradients weights and the variance weights. An offset is added to make the weights positive:

~~$weights = \log10(weights_{Grad} + weights_{Var}) + |\min(\log10(weights_{Grad} + weights_{Var}))|$~~ ~~(1)~~

~~Where~~ $\Omega(t,z) = \log10(\Omega_{Grad}(t,z) + \Omega_{Var}(t,z)) + |\min(\log10(\Omega_{Grad}(t_{all},z_{all}) + \Omega_{Var}(t_{all},z_{all})))|$ (2)

The offset is calculated taking the absolute minimum ~~is taken for~~of Ω over the whole day and at all altitudes. The value of ~~$weights_{Grad}$~~ Ω_{Grad} is given by the inverse negative of the signal gradient ~~value~~ ~~∇S~~ , ∇S . The weights corresponding to positive or zero values of ∇S are set to 1000 times the largest weights of the inverse

negative gradient values so that the cost of choosing a positive gradient is extremely high. The value of ~~$weights_{Var}$~~ Ω_{Var} is given by the inverse of the signal variance~~.~~ $VAR(S)$.

For the KSE site the weights are ~~obtained by the same as equation (1), but~~calculated without the contribution of $VAR(S)$. In fact the ~~variance, because, due to the slant path~~ $VAR(S)$ is large when *S* becomes noisy and shows a larger maximum at the noisy ranges instead at the ~~higher noise already within the CBL we preferred not to use~~CBLH. Because at KSE the signal ~~variance as a weight~~is measured along a slant path, the noise is higher at lower altitudes compared to a vertical measurement (statistically over the entire dataset the SNR < 3 already at 850 m a.g.l.).

~~$weights = \log10(weights_{Grad}) + |\min(\log10(weights_{Grad}))|$~~

Already within the CBL, the value of $VAR(S)$ in eq. (2) could lead to an incorrect retrieval of the CBLH, for this reason eq.(3) is used instead ,

$$\Omega(t,z) = \log10(\Omega_{Grad}(t,z)) + |\min(\log10(\Omega_{Grad}(t_{all}, z_{all})))| \quad (3)$$

~~3.2.5~~4.2.5 Shortest path

~~From sunrise (midnight KSE) to the end of the time series, over consecutive windows of 30 minutes (overlapping at the first and last time steps), the~~The shortest path in a graph (the geodesic in the metric space defined by the weights) ~~are~~is calculated ~~with~~using the Dijkstra's algorithm (Dijkstra, 1959~~), following~~) and is based on the original method ~~of~~described by de Bruine et al. (2016). The Ω-weighted graph is constructed using the signal profiles starting from ~~the matrix representation of the timeseries, the~~sunrise (midnight at KSE) over consecutive intervals of 30 minutes (overlapping at first and last time steps) till sunset (23:59:59 at KSE). Within the lower and upper altitude ~~restrictions and~~limits, the ~~weights. The~~ graph only allows connections of one time step in the positive time direction and ~~jumps~~ of maximum 37.5 m (75 m KSE) ~~amplitude~~ in the altitude direction. ~~A new~~Every shortest path starts ~~where~~ at time t_i when the previous shortest path has ended. In case ~~the previous of failure of~~ shortest path ~~failed~~calculation, the corresponding time window is skipped, and the next shortest path starts at ~~the range of~~(t_i, *z*) corresponding to the first local ~~minimal~~minimum weight. At the first time step (sunrise ~~and~~for PAY, midnight for ~~PAY and~~ KSE~~, respectively~~), the CBLH is set at the ~~inferior graph limit and at the~~ first local minimum weight ~~at PAY and KSE, respectively.~~and constraint by the lower graph limit . The CBLH time series calculated after sunset at PAY is discarded ~~(for PAY).~~

~~3.2.6~~4.2.6 ~~Quality~~ Ratio quality check

~~A~~The retrieved CBLH is checked for quality at each time step by a binary quality index (0/1~~) is set for each time step of the retrieved CBLH time series.~~), where 0 corresponds to no CBLH detection. In case of rain or fog ~~(information directly given by the ceilometer),~~, the quality index is set to 0. ~~Else,~~For all the other sky conditions in order to perform a quality check we calculate the ratio of the mean ceilometer signal over 150 m above the CBLH ~~and~~to the mean ~~ceilometer~~ signal over the 150 m below the CBLH ~~is calculated (the distance to the inferior graph limit is taken if it is less than 150 m). If this.~~ When the ratio is larger than 0.85 (i.e. the signal drop

Formatted: English (U.S.)

Formatted: English (U.S.)

Formatted: Justified

Formatted: English (U.S.)

Formatted: Font: Italic

is less than 15%), the quality is set to 0, ~~else it~~otherwise is set to 1.~~This quality check procedure is similar to what is done by de Haij et al.,(2010).~~

~~3.3~~4.3 Example of PathfinderTURB's TCAL and CBLH calculation

~~For the retrieval of the CBLH, PathfinderTURB uses the backscatter profiles *S* (Eq. 3, sect. 4.2) generated at each time step by the ceilometer.~~ The retrieval's procedure ~~is the following~~of TCAL and CBLH can be summarized in three phases: pre-processing of *S*, CBLH and TCAL retrieval, and quality-check. In the pre-processing ~~step~~phase, $\nabla \log_{10}(S)$, *liminf* and *limphys* are calculated. In ~~step~~phase two, the ~~timeseries~~time series of the range-restricted $\nabla \log_{10}(S)$ is transformed into a weighted graph and the CBLH is determined as the geodesic calculated using the Dijkstra's algorithm (Dijkstra, 1959) within predefined successive subintervals during the temporal interval between sunrise and sunset. Finally, in ~~step~~phase three, the quality of the CBLH retrieval is assessed ~~based on~~using the ~~signal~~ ratio ~~criterion~~quality check.

Based on ~~the described retrieval of~~ equations (2)-(3), the geodesic can be calculated in the metric space defined by the weights~~.~~. PathfinderTURB ~~follows the minima in the vertical aerosol gradients over~~calculates a ~~sequence of retrievals. The way the geodesic is calculated limits the problem of~~line connecting the (t_i, *z*) pairs that minimize the cost function defined by the weights. The connecting line is the geodesic and has the property to strongly reduce the occurrence of unphysical jumps between different layers when boundaries disappear or reappear~~. In this work,~~ due to real atmospheric dynamics. PathfinderTURB ~~has been extended from the original pathfinder to use the signal variance in~~ uses $VAR(S)$ in addition to ~~the aerosol gradients. Based also on Equation (1), PathfinderTURB combines the information provided by the gradient with that provided by the variance. As a result, regions with high signal variance are favoured in the CBLH~~ ∇S in order to solve the attribution ~~process, which yields a physically~~ problem in a more ~~robust detection. This~~physical way identifying regions characterized by large values of $VAR(S)$ and using it to retrieve the CBLH. The CBLH is ~~accomplished by multiplying the gradient based weights of the graph by the inverse of the atmospheric variance value.~~attributed to a layer's boundary in (t_i, *z*) when this point minimizes the cost function, i.e. minimizes the term $COST = \Omega_{Grad} \times VAR(S)^{-1}$. In this way, the influence of artificial and static aerosol gradients, present in some models of ceilometers and due to an incorrect overlap correction, is largely reduced. The different steps of the PathfinderTURB algorithm are illustrated in Figure ~~1~~2, in four ~~timeseries~~time series (panels a, b, c and d) for the case of 15 July 2014 in PAY.

In ~~panel a),~~Figure 2a, the logarithm of the range-corrected signal is displayed. The cloud base height (CBH) is directly provided by the ceilometer manufacturer's software and displayed in grey throughout all ~~the~~ panels. The TCAL ~~is (~~shown in green ~~throughout all the panels. As already introduced above (Sect. 3.1), the TCAL)~~ is the combination of the altitudes determined by applying the *signal condition* and the *SNR* ~~conditions~~*condition* (sect. 4.1) plus the height of the first cloud layer. The *signal condition* and the ~~height of the first cloud layer~~ CBH play a critical role in this example. ~~In panel (a),~~The development of the CBL is ~~restricted~~ limited in altitude by the TCAL, but it can also be ~~restricted furthermore~~limited below the TCAL by ~~additional physically meaningful~~

Formatted: Font color: Black

Formatted: Font: Italic

Formatted: Font: Italic

~~altitude limitations (~~the other limits contributing to *limphys*~~), displayed in magenta. These~~ (sect. 4.2.2). The *limphys* ~~depend on climatology~~is the minimum height amongst the climatological, the TCAL, the CBH and ~~the height~~that of strong negative and positive gradients (~~which indicate~~indicating mixing discontinuities). ~~Strong~~ During the period 02:00-03:30 UTC, *limphys* (magenta) was determined by strong positive gradients ~~can be observed in panel (a)~~ at about 1500 m a.s.l~~. between 02.~~.; during 20:00-24:00 UTC and ~~03:30 UTC;~~at about 1750 m a.s.l.by strong negative gradients~~ occur at about 1750 m a.s.l. between 20:00 and 24:00 UTC~~.

In ~~panel b),~~Figure 2b, the ~~variance~~ $VAR(S)$ is displayed. ~~The variance~~ $VAR(S)$ is calculated using spectral analysis, more precisely is the result of integrating the spectrum of band-pass filtered, one-hour-long *S*-~~timeseries~~time series at each altitude (as in Pal et al., 2013). The band-pass filter aims at removing mesoscale and noisy fluctuations so that only fluctuations due to short-lived aerosol load variability are taken into account (Supplement S2). The ~~minimum~~lower altitude ~~limitation~~limit (*liminf*) is calculated ~~from there~~based on the $VAR(S)$ value, and displayed in magenta. ~~Indeed, the entrainment occurring~~The next region of enhanced $VAR(S)$ above *liminf* corresponds to the EZ at the top of the CBL~~ prevents~~, the fact of preventing the retrieval to include the region [0- *liminf*] helps locating correctly the CBLH~~ to be located below this first region of enhanced variance~~.

In ~~panel c),~~ Figure 2c, the weights $\Omega(t,z)$ are displayed. ~~Using the Dijkstra's algorithm, PathfinderTURB calculates~~Based on equations (2), (3) the CBLH~~ as the most cost efficient~~ path ~~from sunrise to sunset (black line), i.e. the CBLH path tends to follow~~follows the deep-blue regions ~~(low weights)~~corresponding to a minimum in ~~the timeseries of weights.~~ $\Omega(t,z)$. The path can only follow the positive time direction and altitude changes are limited to 0.625 m/s. ~~The weights are given by the product of the inverse magnitude of negative gradients and of the variance values (sect. 3.2.4). Thus, the top of the CBL, which~~ The CBLH is characterized by a drop in the aerosol concentration (large negative ∇S) and high entrainment activity (~~and thus high variability), will most likely have a low weight.~~large $VAR(S)$), which corresponds to minimum $\Omega(t,z)$.

In ~~panel d),~~Figure 2d, a final overview is given, with the retrieved CBLH (black line) displayed on top of the log10(*S*) ~~timeseries~~time series, together with the TCAL and the ~~cloud bases~~CBH.

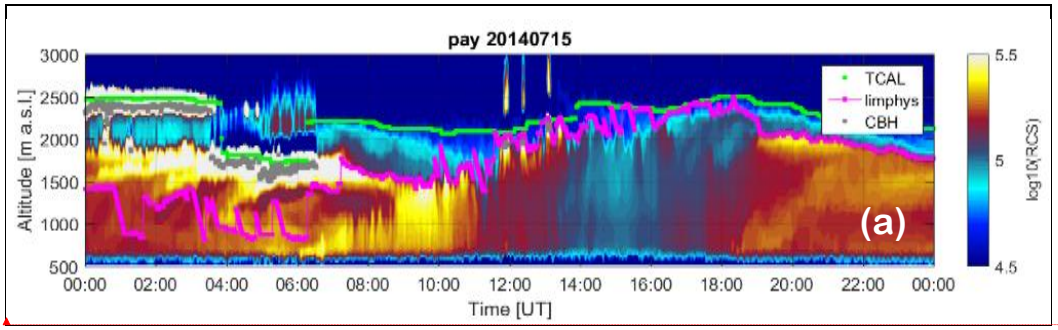

Formatted: Font color: Auto

Formatted: Font color: Auto

Formatted: Font: 12 pt

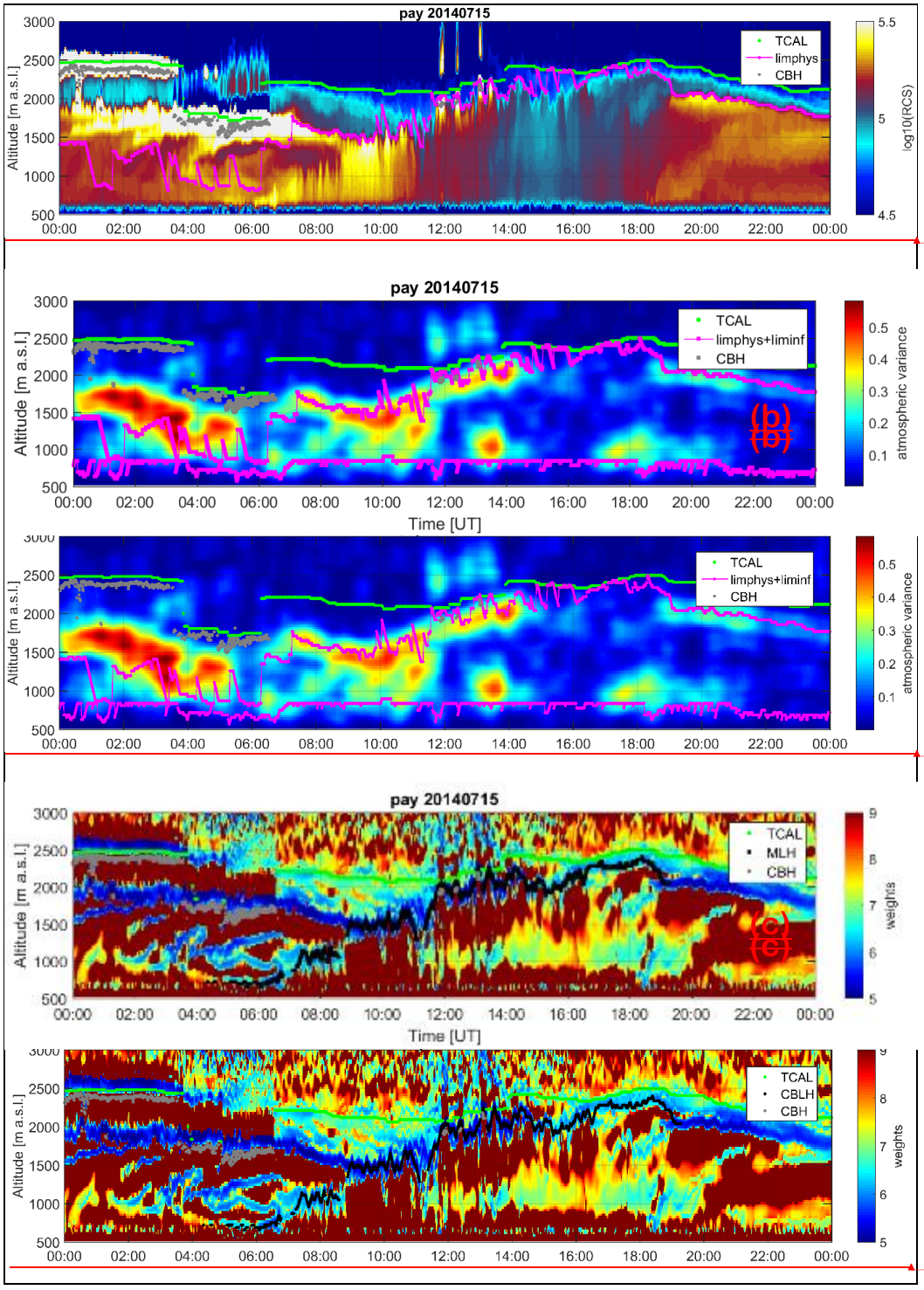

Formatted: Font: 12 pt

Formatted: Font: 12 pt

Formatted: Font: 12 pt

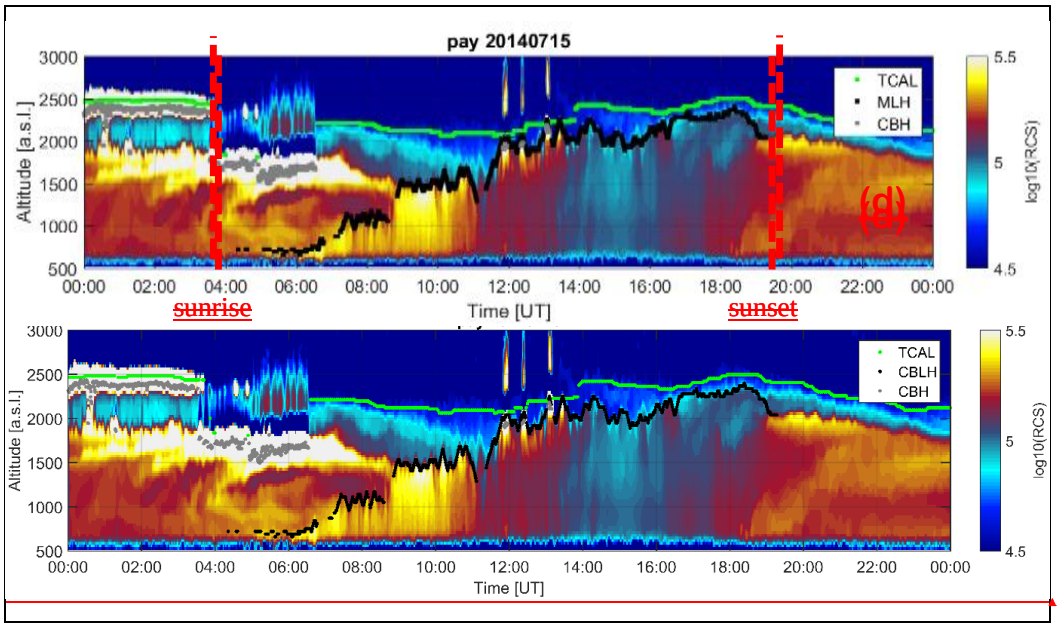

Figure ~~1: Timeseries~~2. Time series of the different processing steps of the PathfinderTURB ~~algorithm~~ for 15 July 2014 ~~in~~at PAY. Panel a) ~~timeseries~~time series of log10(*S*) with ~~the~~superimposed TCAL, ~~the cloud bases~~CBH and ~~the superior limit (*limphys*)~~ for altitude. Panel b) ~~Atmospheric variance, cloud bases~~time series of $VAR(S)$ with superimposed CBH, *limphys*, ~~inferior limit~~*liminf* for altitude ~~(*liminf*).~~. Panel c) ~~Weights,~~time series of $\Omega(t,z)$ with superimposed TCAL, ~~cloud bases~~CBH and retrieved ~~MLH~~CBLH (geodesic from sunrise to sunset). Panel d) ~~timeseries~~time series of log10(*S*) with ~~the~~superimposed TCAL, the ~~cloud bases~~CBH and the retrieved ~~MLH~~CBLH.

Formatted: Font: 12 pt

Formatted: English (U.S.)

~~4 Remote sensing and in-situ observations at Payerne and Kleine Scheidegg~~

~~Two CHM15k ceilometers were installed at two different sites in Switzerland. The first at PAY in a rural and comparatively flat environment. PAY is equipped with numerous meteorological measurements allowing to interpret and to validate the measurements from the ceilometer. The most relevant measurements in the framework of the presented study are: a Raman LIDAR measuring humidity, temperature and backscatter at 355 nm and at the Raman-shifted wavelengths (Dinoev et al., 2013; Brocard et al., 2013), a wind profiler (Degreane, 1290 MHz), a RPG-HATPRO microwave radiometer measuring temperature and humidity using 14 channels around the water vapour and oxygen absorption lines, the operational Meteolabor SRS-C34 radiosondes launched twice daily at 00 and 12 UTC (Philipona et al, 2013), the sun photometers (direct, diffuse and global short and long wave, Vuilleumier et al., 2014) and the surface sensors of temperature and humidity.~~

~~A second instrument was installed at KSE, close to the JFJ. The JFJ is part of numerous global observation programs like GAW (Global Atmospheric Watch), EMEP (European Monitoring and Evaluation Programme), NDACC (Network for the Detection of Atmospheric Composition Change) and AGAGE (Advanced Global~~

Atmospheric Gases Experiment). Most importantly, in the context of this this work, JFJ participates with in-situ observations as a level-1 station in the ICOS project. In contrast to other ICOS sites located over flat terrain, it was decided to install the ceilometer at KSE to characterize the CBL below and above the JFJ. The presence of aerosols, detected by the ceilometer, and the frequency at which these reach the JFJ, can be directly compared with the chemical and physical in-situ measurements of aerosols and trace gases at the JFJ. In fact, several in-situ instruments are installed at the JFJ and operate continuously since many years to measure optical and chemical properties of aerosols and trace gases as well as diverse meteorological parameters (Bukowiecki et al., 2016). Instruments of direct interest to our study are: a condensation particle counter (CPC; TSI Inc., Model 3772), which measures the particle number concentration and two instruments providing aerosol absorption coefficients: a Multi-Angle Absorption Photometer (MAAP) measuring at 637 nm and an aethalometer (AE-31, Magee Scientific) measuring at seven different wavelengths. The aerosol in-situ measurements are performed under dry conditions (relative humidity <20 %), while the ceilometer probe the unmodified atmospheric volume.

4.11.1 Sites description

The PAY site (Figure 2) is situated in the centre of the Swiss Plateau between the Jura Mountain range to the north-west (at a distance of 25 km) and the Alpine foothills to the south-east (20 km). The measurement site is characterized by a rural environment leading to biogenic aerosols sources combined with moderate urban emissions characterized by anthropogenic aerosol sources especially related to cars exhaust and house heating.

The KSE (Figure 2, KSE) is located in the Bernese Oberland Alpine region, at an altitude of 2069 m. It can be seen as a saddle point between the mountain peak Lauberhorn (2472 m) to the northwest and the Jungfraujoch (3465 m) to the southeast, and it is a pass between the villages of Wengen and Grindelwald. This topographic configuration has a considerable influence on the local wind circulation. Winds at the KSE are mostly blowing along the SW-NE axis (Ketterer et al., 2014), whereas the prevailing wind at JFJ are from NW toward SE. The JFJ itself is located on the ridge formed between the Mönch and the Jungfrau mountains and is 4.5 km to the south-east and 1.5 km higher than KSE. Most of the atmospheric observations at the JFJ are obtained at the Sphinx observatory (3580 m a.s.l.).

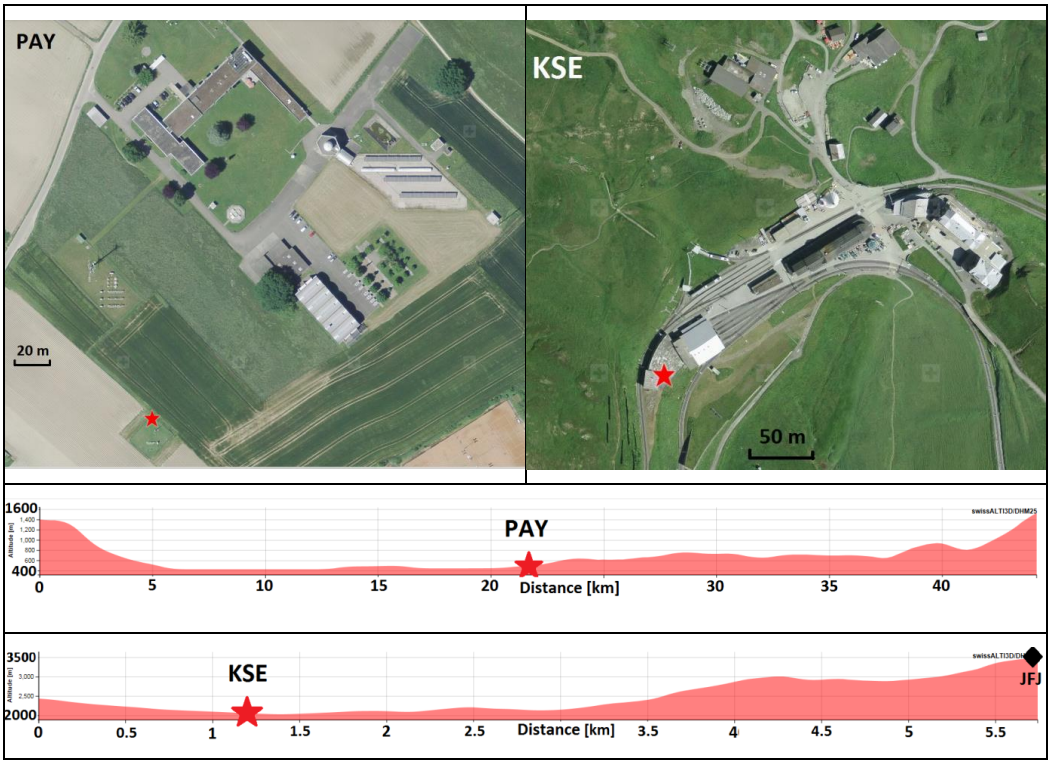

Figure 2: Aerial view and topography of PAY (elevation profile along the 127.2° Azimuth), and KSE (elevation profile along the 151.6° Azimuth) as provided by the federal office of topography (http://www.geo.admin.ch/). The red stars mark the position of the ceilometers at PAY and KSE, the black diamond marks the JFJ position.

4.2 CHM15k Ceilometer data and settings

The measurements from a ceilometer of type CHM15k-Nimbus (hereafter referred to as CHM15k) manufactured by Lufft have been used for this study. The CHM15k is a bistatic LIDAR with a Nd:YAG solid state laser emitting linearly polarized light at a wavelength of 1064 nm. It has a repetition rate ranging between 5 and 7 kHz, a maximum vertical resolution of 5 m, a maximum range of 15 km, a first overlap bin at 80 m and a full overlap reached at 800 m (specific for KSE, and PAY ceilometers, Hervo et al., 2016). The standard instrument output is a function of the received power per laser pulse, P, backscattered by the atmosphere at range r and time t. More precisely, the standard output of the CHM15k is the background, range and overlap corrected, normalized signal, S defined as:

$$S = \frac{(P(r,t) - B(t))r^2}{C_{CHM}(t)O_{CHM}(r)} \quad (3)$$

Where, B is the background, C_{CHM} is a normalization factor accounting for variations in the sensitivity of the receiver and O_{CHM} is the temporally constant overlap function provided by the manufacturer.

~~The measurements used for this study have been collected during the period January-December 2014 at PAY and during September 2014 – November 2015 at KSE. At PAY, the ceilometer was setup vertically with a slight tilt (5° zenith angle) to avoid the specular reflection effect on cirrus ice crystals, as suggested by the manufacturer. At KSE, the ceilometer was mainly operated in tilted setup (71° zenith angle) in order to point towards the JFJ. At both sites, the overlap function O_{CHM} has been corrected for temperature variations following (Hervo et al., 2016).~~

Formatted: Heading 2

~~4.2.1 1.1 Special instrument settings for KSE~~

~~The CHM15k ceilometer at KSE was installed in August 2014 on the roof of the maintenance centre of the train station, at an altitude of 2069 m (Figure 2). From September to November 2014 and from March to November 2015, the ceilometer was tilted at 71°zenith angle with the laser beam passing close above (~20 m) the JFJ. From the beginning of November 2014 till the end of February 2015, the ceilometer was set back in the vertical position (5° zenith angle) to prevent the sun shining directly onto the ceilometer's telescope.~~

~~The tilted setup of the ceilometer was chosen to observe the injections of CBL air at the level of JFJ and to probe the same air that is measured by the in situ instruments at the JFJ. The tilted configuration has required an adjustment of the heater to redirect the heat flow inside the CHM15k case and prevent the overheating of the laser. Moreover, when measuring in slant path the maximum vertical height, R_{max}, depends on the tilt angle and on the instrument's maximum range (15 km for the CHM15k), then, when measuring at 19°elevation angle $R_{\max} = 2.069 + 15\sin(19°) = 6.64$ km a.s.l.. At this relatively low altitude, the standard background correction that subtracts from the received power P its own mean value over the *far range* (furthest ranges along the profile, where the signal is assumed to be entirely represented by noise), cannot be performed as the far range may still contain aerosols or clouds. In order to overcome this problem a new technique of background removal that depends on the variance of P has been developed and applied to each profile. The variance is calculated within spatial windows of 120 m to 1600 m (in steps of 120 m) and computed for all range bins between 390 m and 14970 m. The background corresponds to the mean value of P over an optimal window. The optimal window's position is the one minimizing the average of its variance values. The optimal window's width is the one corresponding to the 75th percentile of the variance values at the optimal window's position. Another advantage of measuring in slant path is that, compared to the vertical setup, the JFJ is reached by the ceilometer's laser beam at 4.8 km that is already in the full overlap region.~~

5 PathfinderTURB validation at Payerne

Although, gradient-based algorithms are easy to implement for automatic operations, the layer attribution remains the main ~~limitation for the retrievals. Normally, most of the uncertainty affecting a CBLH retrieval depends almost solely on the choice of the best gradient. We believe that for~~source of uncertainty of the retrievals. For methods based on aerosol gradients the visual identification of the correct gradient by human expert still solves the attribution problem with the least uncertainty. Therefore, PathfinderTURB is validated here against independent detections by human experts as well as against the bulk-Richardson method applied to co-located radiosonde profiles. The aim of the validation is to create an as-accurate-as-possible reference without selecting only golden-cases, but filtering out those cases when fog and precipitation prevent to define the CBL.

5.1 Comparison with Human expert CBLH retrieval

A graphical user-interface has been developed for the human experts to detect the CBLH manually by clicking on the time-height cross section of *S*. Auxiliary information are available from the interface about ~~∇S (central differences ($S(r_{i+1},t_j) - S(r_{i-1},t_j)$)/(2Δr)), the temporal variance~~ ∇S ; $VAR(S)$ (over 10 minutes~~), the~~); sunshine duration, ~~the~~ vertical heat flux at the surface~~, the;~~ trend of hourly-averaged surface temperatures ΔT~~, the;~~ hourly stability index (as defined in Pal et al., 2013~~), the~~); sunset/sunrise time~~,~~; estimations of the CBLH based on the Parcel method (PM, Holzworth, 1964) and the bulk Richardson method (*bR*, Richardson, 1920) from continuous remote sensing instrumental data (Microwave Radiometer, Wind Profiler, Raman LIDAR), and twice daily radiosounding data (at noon and at midnight). The experts perform a manual detection of the entire daily cycle with the support of all the ancillary data and information.

Four experts from the remote-sensing division of MeteoSwiss have processed ~~the overlap-corrected, normalised signal, *S*,~~one year of data ~~from~~(2014) of the PAY CHM15k ~~for Payerne for the year 2014~~. The guidelines and the criteria of the manual CBLH detection are provided in the Supplement (S5).

5.1.1 Analysed dataset

We compared the detections by three experts (*test group*) against one expert that ~~is called the~~acted as *reference*. For the year 2014, the analysed days were the 5th, 10th, 15th, 20th, 25th and 30th of each month and the whole months of January, March, July and October~~; the~~. The *test group* analysed the 5th, 10th, 15th, 20th, 25th and 30th of each month. Once the missing data (due to instrument disruptions) and fog or precipitation days had been removed from the dataset, the total number of days analysed was 174. Covering an entire year, the database inspected by the *test group* and the *reference* is comprehensive in terms of diverse synoptic conditions, sunshine duration, cloudiness~~,~~ and season~~, etc~~. The ~~ceilometer~~ *S*-profiles were analysed by the ~~experts of the~~ *test group* separately and with no possibility to ~~interact with~~influence each ~~other.~~other's choice. The detections made by the *reference* ~~("reference data")~~ and those made by the *test group* were compared at each time step so that a matching procedure was established between a CBLH point in the *reference* ~~data~~ and the *test group*'s detections for the same time step. Only the CBLH points that ~~match~~matched in time were retained for the comparison. If needed, the *test group* detections were linearly interpolated in order to match exactly the time vector of the *reference*. When comparing the *reference* ~~data~~ with all the *test group* detections the two datasets showed an excellent agreement, with a coefficient of determination ~~equal to~~of 0.96 (total of 5097 points over 140 days) and RMSE of 92 m. Nevertheless, some large difference (> ~~500m~~500 m) in the CBLH detections occurred in less than 3 % of all cases. In general, discrepancies occurred when there was more than one layer that could be reasonably followed as CBLH, for example when an advected aerosol layer ~~enters~~entered the profile and ~~gets~~got mixed inside the CBL or during the often ambiguous separation between the RL and the decaying CBL in the afternoon after the convective peak.

~~5.1.2 Determination of the expert consensus~~

~~The CBLH detections by each expert are linearly interpolated over 30 s and truncated before sunrise and after sunset. Before comparing the CBLH values retrieved by PathfinderTURB with those detected by the experts, a~~

Formatted: Font: Italic, Font color: Black

Formatted: Font color: Black

Formatted: Font: Italic, Font color: Black

Formatted: Font color: Black

number of additional restrictions are defined. Manually-detected CBLH values for a given day must fulfil the following conditions in order to be "valid":

- No precipitation (station measurement) and no fog (ceilometer measurement) for more than 2 consecutive hours.
- Only time periods of at least 30-minute duration, containing interpolated data from at least 2 experts and with spread (i.e. difference between the maximum and minimum values) of less than 10% of the mean CBLH plus 100 m are taken into account. The allowed spread increases with altitude because the probability to lie on different layers decreases with increasing altitude. The offset of 100 m added to the maximum allowed spread is an empirical value that translates into a permitted 300 m spread for a CBLH at 2000 m, which is a conservative estimate of the depth of the entrainment zone at that altitude (EZ depth can be 40% of the CBLH, Stull, 1988).

The CBLH detections respecting the above criteria are retained for comparison with PathfinderTURB. The mean value of all the valid detections (*reference* and *test group*) for each time step was calculated along with the lower and upper error bounds determined as the minimum and the maximum CBLH detections. In total, an expert consensus was reached for 135 days, out of the initial 174, covering a total of 43914 minutes. On 6 days, no ceilometer data were available. On 13 days, poor weather conditions prevented all detections. On 20 days, either the spread was too large or the duration of the matched temporal interval was too short.

Because the number of CBLH detections decreases as the days become shorter in winter, midday is the period of the day with the highest availability of detections (and the best agreement). Both morning and afternoon periods present difficulties, when detecting the CBLH from the timeseries of *S*, nevertheless the morning provides better availability of detection than the afternoon. The limitations of morning detections are related to the fact that during the first 2-3 hours after sunrise the CBL top is still low above the ground (< 200 m a.g.l.) and the overlap-corrected, normalized signal, *S*, is affected by the incomplete overlap in that zone, which makes the detection in the first few hundred meters difficult and more uncertain. Another source of complexity in the morning detections is that the residual nocturnal layer may remain aloft and very close to the developing CBLH, which increases the uncertainty related to the layer attribution. During the late afternoon, the CBL transforms into the RL as soon as buoyancy weakens and it becomes neutrally stratified. Under these conditions, the CBL top drops rapidly, but usually without displaying a clear aerosol gradient, which leads to a large (and somewhat unphysical) spread among the experts' detections.

5.1.35.1.2 PathfinderTURB validation against the expert consensus

After applying the ratio quality check (sect. 34.2.6) to the PathfinderTURB retrievals, the total number of the accepted retrievals covers 34720 minutes out of the 43914 minutes of obtained by the manual datadetections, i.e. 79% of the human expert consensus. In other words,The ratio quality check of PathfinderTURB removes about the 20% of itsthe retrievals because of weak gradients at the level of the retrieved CBLH. The validated PathfinderTURB retrievals that passed the quality check are spreaddistributed over the same number of days, (i.e., 135). Figure 3 shows, for Payerne and) during the year 2014.; the top panel of Figure 3 shows the density scatter plot of the CBLH values obtained at PAY by the human experts' detections meeting the (consensus and

~~by~~) manual detections versus PathfinderTURB ~~(top panel), and the~~ . The boxplot ~~plus~~along with the histogram ~~(~~shown in the bottom panel~~) of~~ display the differences between the two data sets. A coefficient of determination of 0.96, an RMSE of 76 m and an interquartile range of the differences of 96 m are obtained. The median and mean ~~difference~~differences are 27 m and 41 m, respectively. The overestimation is largest during the second half of the afternoon (not explicitly shown here), when PathfinderTURB tends to follow the top of the residual layer instead of the decaying CBL. Furthermore, the error is smaller than 500 m for 98.6% of the PathfinderTURB retrievals, and 92% of the retrievals have a relative error (~~w.r.t~~with respect to the ~~manually determined~~manual CBLH) smaller than 10%.

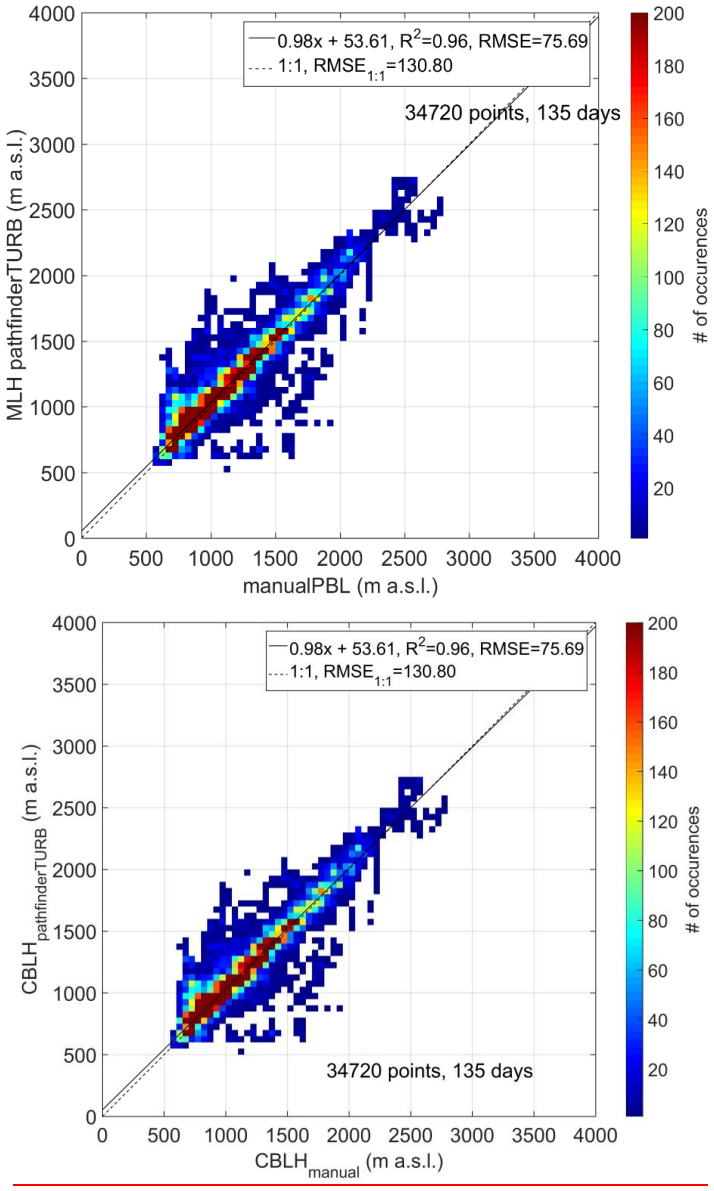

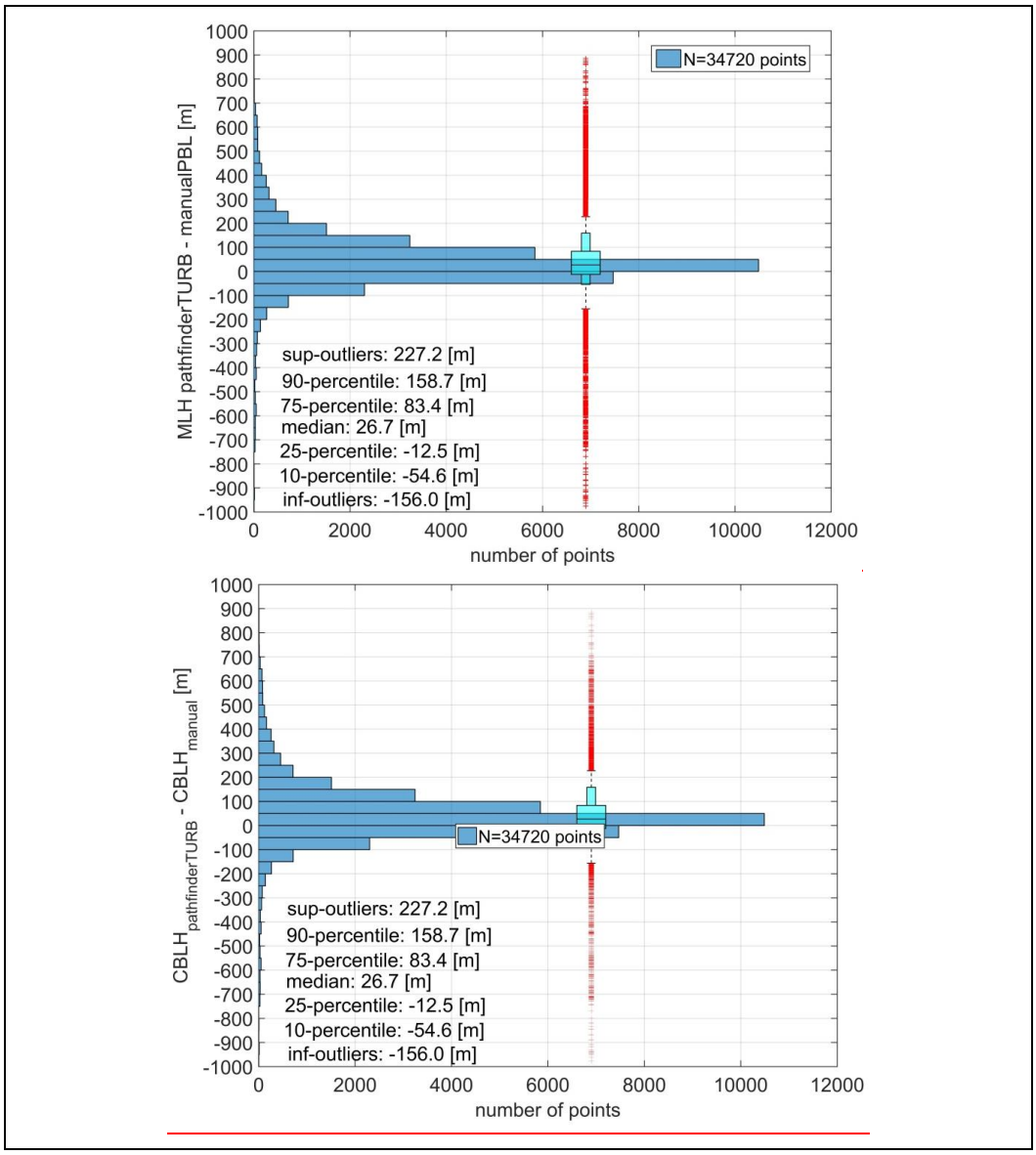

Figure 3~~ top panel shows the density~~. Density scatter plot of ~~PathfinderTURB~~$CBLH_{PathfinderTURB}$ vs. ~~manualPBL. The bottom~~$CBLH_{manual}$ (top panel~~ shows the boxplot~~). Boxplot and histogram of the difference between the PathfinderTURB and ~~manualPBL.~~manual datasets (bottom panel).

The comparison shows that PathfinderTURB is robust ~~(no unphysical jumps, cloud presence taken into account) and~~and that can address the attribution problem adequately. Although PathfinderTURB combines both gradient and variance methods to improve the correctness of the retrieval in different atmospheric conditions, the retrieval's uncertainty grows larger during the afternoon due to the ~~convective~~ decay of convection before

sunset, the weak turbulence and the lack of well-marked aerosol gradients. During this period, temperature or vertical wind variability profiles may provide more valuable information than ceilometer ~~data~~profiles.

5.2 Comparison with radiosonde-estimated CBLH

~~Next, the~~The PathfinderTURB retrievals of the CBLH were compared to the retrievals from two methods based on the thermal structure of the atmosphere: the PM and the *bR*. The PM defines the ~~upper boundary of the CBL~~CBLH as the height to which an air parcel with ambient surface temperature can rise adiabatically from the ground, neglecting other factors (entrainment/detrainment, advection, subsidence, air humidity). It relies on profiles of potential temperature (Θ) and therefore requires vertical profiles and surface values of temperature (T) and pressure (p). In Payerne, Θ profiles are generated every 10 minutes by a microwave radiometer (MWR), and at noon and midnight also by RS. The bulk Richardson number (Ri_b) is a dimensionless parameter that can be seen as the ratio between the buoyancy and the wind-shear generated turbulence. The ~~upper boundary of the CBL~~CBLH is determined as the first height where Ri_b exceeds the critical threshold of 0.33 (unstable conditions) or of 0.22 (stable conditions). The required input values are the profiles of Θ and the wind. The stability conditions, essential for choosing the correct threshold value, are derived from the sign of the slope of the linear fit of Θ in the first 30 m. At Payerne, wind profiles are provided every 30 minutes by the wind profiler (WP), and at noon and midnight also by RS. ~~As the threshold value is larger than zero, the *bR* method retrieves higher CBLH values than the PM.~~ We refer to Collaud Coen et al. (2014) for a more detailed description of the operational CBLH retrievals at Payerne using the *bR* method.

PathfinderTURB is compared to the RS-based *bR* ~~retrieval~~retrievals of the noon CBLH during the year 2014. In order to increase the robustness of the *bR* retrievals, the comparison is performed only when both *bR* and PM retrievals are available. Based on the calculations of Collaud Coen et al. (2014) the uncertainty of the retrieved CBLH using both methods is on the order of ±50 to ±250 m for the midday peak of the CBLH. Within their uncertainty intervals, the two methods can then be considered providing the same retrievals when the difference between them is equal to or less than 250 m. For this reason only the retrievals ~~being~~matching closer than 250 m and ~~having~~with an uncertainty of less than 250 m have been retained for the comparison. That has resulted in a total of 175 days being considered. ~~Out of the 365~~Of these 175 days ~~considered, the ceilometer data at noon were not available~~ only on ~~16~~115 days~~. Of the remaining 349 days,~~ PathfinderTURB ~~has been able to~~could retrieve ~~the~~a valid CBLH ~~on 202 days (58%). Out of the 202 days, 115 days (31.5%) had both *bR* and PM~~. Thereafter and for simplicity, only the *bR* retrievals ~~satisfying the robustness conditions listed above~~will be used in the comparison with PathfinderTURB (*bR* and PM pairs were always available for the considered 115 days).

The median and mean difference between RS~~-~~ and PathfinderTURB ~~retrieved~~ CBLH ~~was~~values were 53 m and 41 m, respectively, indicating a slight overestimation of the *bR* method with respect to PathfinderTURB. From the comparison we obtain a coefficient of determination of 0.85, a regression slope of 1.02 (~~Fig.~~Figure 4, top panel), an RMSE of 162 m and an interquartile range of the difference of 174 m, ~~hence~~ (larger than the spread observed in ~~the comparison with the human expert retrievals.~~Figure 3). The ~~difference~~ distribution of the differences in Figure 4, bottom panel, has a Gaussian shape~~,~~ with slight positive offset values ~~(Fig. 4).~~ About the 98% of the data have an error smaller than 500 m, and the 82% have an error smaller than the 10% (plus 100

m) of the CBLH ~~retrieval~~retrieved by *bR*. In general, the correlation between PathfinderTURB (ceilometer-based) and the *bR* retrievals (RS-based) is not ~~quite~~ as good as the one between PathfinderTURB and the ~~experts'~~manual retrievals (both ceilometer-based). ~~When comparing~~For the ~~two methods, one using radiosonde and the other the ceilometer data~~comparison shown in Figure 4, it should be remembered that the two methods rely on different physical processes, i.e. thermal structure of the atmosphere (RS) versus actual state of mixing of the aerosols (ceilometer). ~~An example~~A consequence of the different physical processes is the slight overestimation of the *bR* ~~between~~method during the period from the end of ~~the~~ morning ~~and~~till the beginning of ~~the~~ afternoon, i.e. when buoyancy-produced turbulence reaches a maximum. This is because the *bR* indicates the depth of the layer where conditions are favourable for vertical mixing, whereas the aerosol gradient depicts the actual state of mixing. By ~~visual inspection of~~using the MWR data to evaluate the entire daily cycle (not only 12 UTC~~) dataset of comparisons~~ by RS) the comparison PathfinderTURB vs *bR* ~~using the MWR data we conclude~~shows that the *bR*-based CBLH rises generally faster than the aerosol gradient in the morning. The decay of the *bR*-based CBLH occurs also generally faster than that of the aerosol gradient in the late afternoon, resulting in *bR* retrievals lower than the PathfinderTURB CBLH retrievals~~ based on aerosol gradient~~. This is explained by the fact that the aerosols remain suspended in the near-neutrally stratified air (transition from CBL to RL) and that no detectable aerosol gradient forms at the top of the decaying CBL. The gradient remains thus at about the same altitude as its midday maximum leading to a significant overestimation by PathfinderTURB. For this reason, LIDAR and ceilometers using aerosols as tracers are not best suited to detect the CBL decay, but rather the RL. Nevertheless, although at ~~the local noon~~12:00 UTC the *bR* still ~~diagnoses~~provides a slightly higher CBLH, the ~~time when the peak of convection occurs is a suitable time interval when to compare the~~comparison shown in Figure 4 proves a good agreement between *bR* ~~with~~and PathfinderTURB.

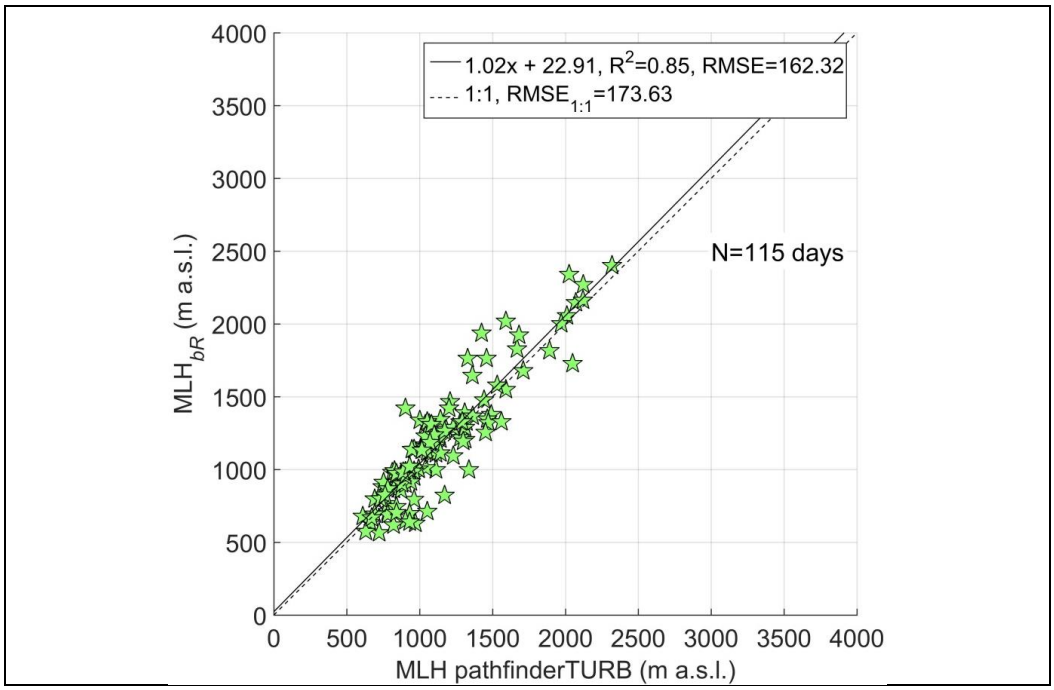

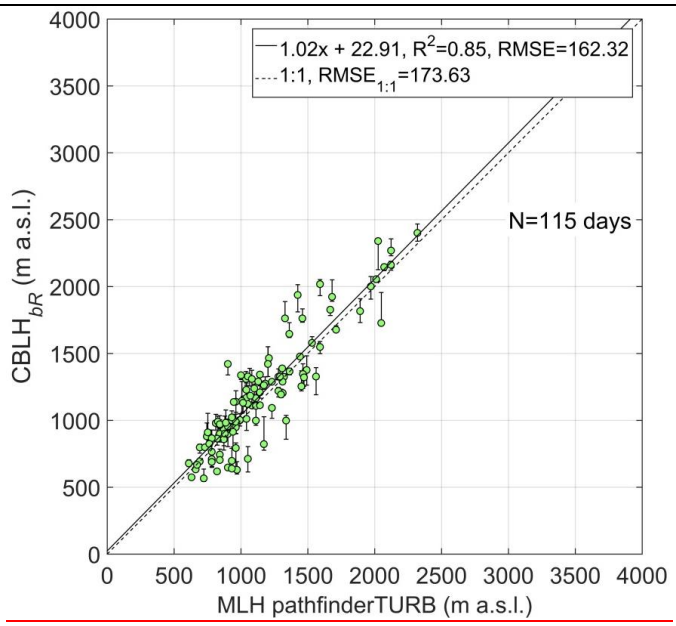
1.02x + 22.91, R2=0.85, RMSE=162.32
1:1, RMSE1:1=173.63
N=115 days
CBLHbR (m a.s.l.)
MLH pathfinderTURB (m a.s.l.)

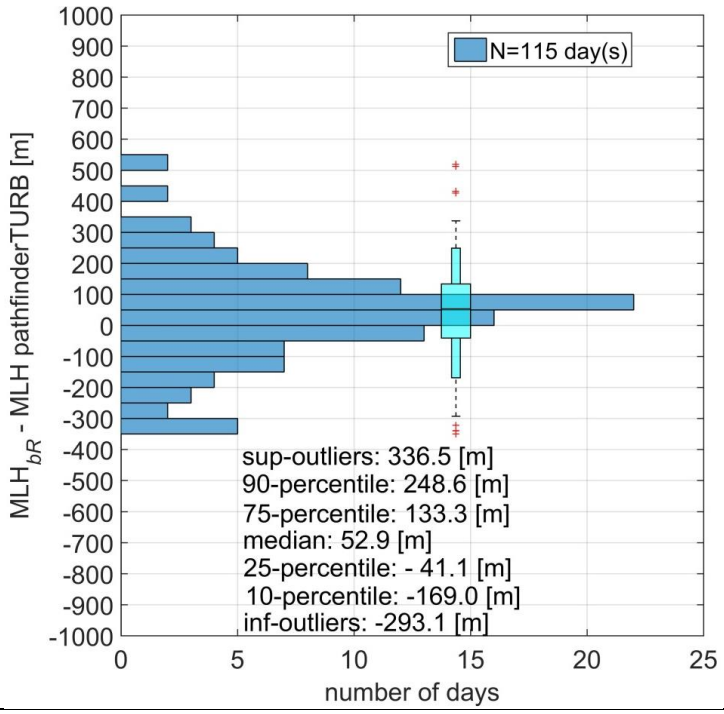
N=115 day(s)
MLHbR - MLH pathfinderTURB [m]
sup-outliers: 336.5 [m]
90-percentile: 248.6 [m]
75-percentile: 133.3 [m]
median: 52.9 [m]
25-percentile: - 41.1 [m]
10-percentile: -169.0 [m]
inf-outliers: -293.1 [m]
number of days

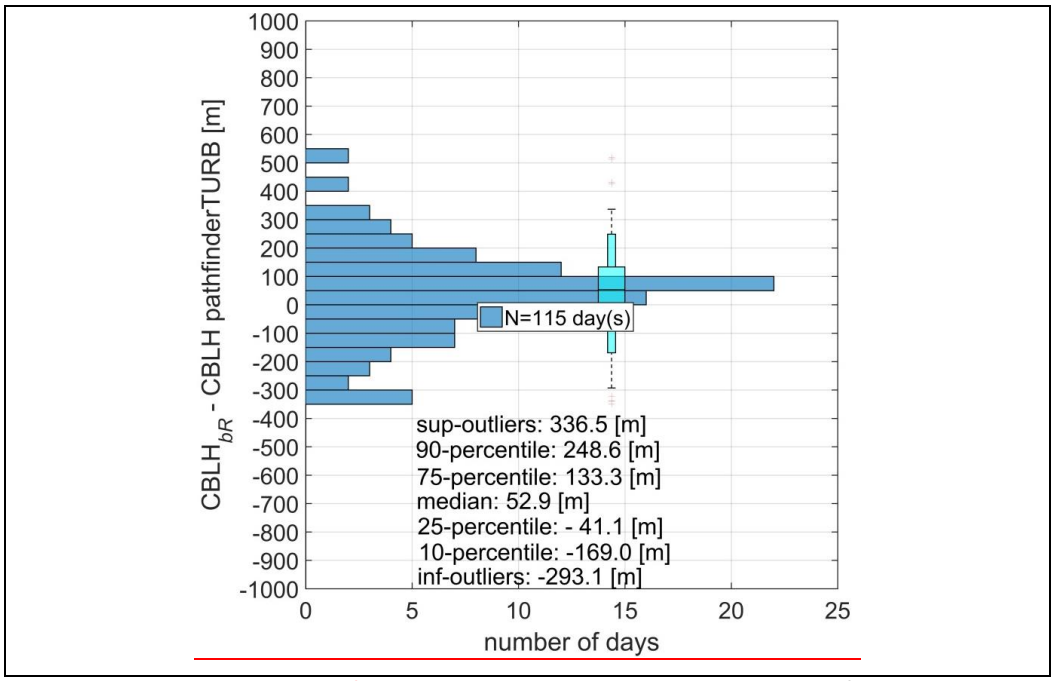

Figure 4~~: the upper~~. all data shown refer to 12:00 UTC. Top panel ~~shows the~~: scatter plot of ~~RS(*bR* 12H)~~CBLH$_{bR}$ vs. ~~PathfinderTURB. The bottom~~CBLH$_{\text{PathfinderTURB}}$. Bottom panel ~~shows the~~: boxplot and histogram of the difference between ~~RS(~~the *bR* ~~12H)~~ and PathfinderTURB~~.~~ datasets.

Formatted: Font: 9 pt

~~6 PathfinderTURB~~Measurements of CBL, CAL and aerosol properties at ~~the Kleine Scheidegg~~

Formatted: Heading 1

~~6.1~~6 ~~Transport of BL air masses to the~~ JFJ

Updrafts and downdrafts (initiated and sustained by solar radiation received at the surface) ~~is~~are the main vertical transport mechanism of the CBL air above the Swiss Plateau (Collaud Coen et al., 2011). Air lifted from a sunlit mountain slope is often warmer than the air at the same height over an adjacent valley even if the latter was lifted from the valley floor. Hence, next to the development of up-slope (anabatic) winds, thermals generated at a mountain slope may rise higher than those generated at the valley floor. When both the topography and the meteorological conditions are favourable, up-slope winds ~~may~~can develop and become strong enough to break through the CBL's capping inversion and inject CBL air into the FT immediately above the local CBL (LCBL) resulting in the formation of an aerosol layer (AL) above the CBL (Henne at al., 2004). This complex mountain circulation is characterized by dynamics occurring at different spatial scales (Figure 5). The AL or *injection layer* is a near-neutral, partly-mixed layer that is more diluted than the LCBL being the result of LCBL air mixed with FT air. The LCBL normally follows the topography (scale of a few kilometres), especially in the morning, and is often topped by a temperature inversion that marks the transition with the above AL. ~~The~~At its upper boundary, the AL does not follow individual valley or ridges, but follows the large-scale topography (few tens of kilometres) and ~~again maybe capped~~can also be overlaid by a temperature inversion ~~that marks~~marking the transition ~~to~~with the FT (Henne at al., 2004, de Wekker, 2002). In his work, de Wekker (2002) concludes that in mountainous regions, the mixing layer height corresponds to the top of the AL rather

than the top of the LCBL and he renames it "mountain mixing layer", because the AL depicts the height up to which particles can be transported by the various venting processes. The combination of the LCBL and the AL forms the CAL~~.~~ (Figure 5).

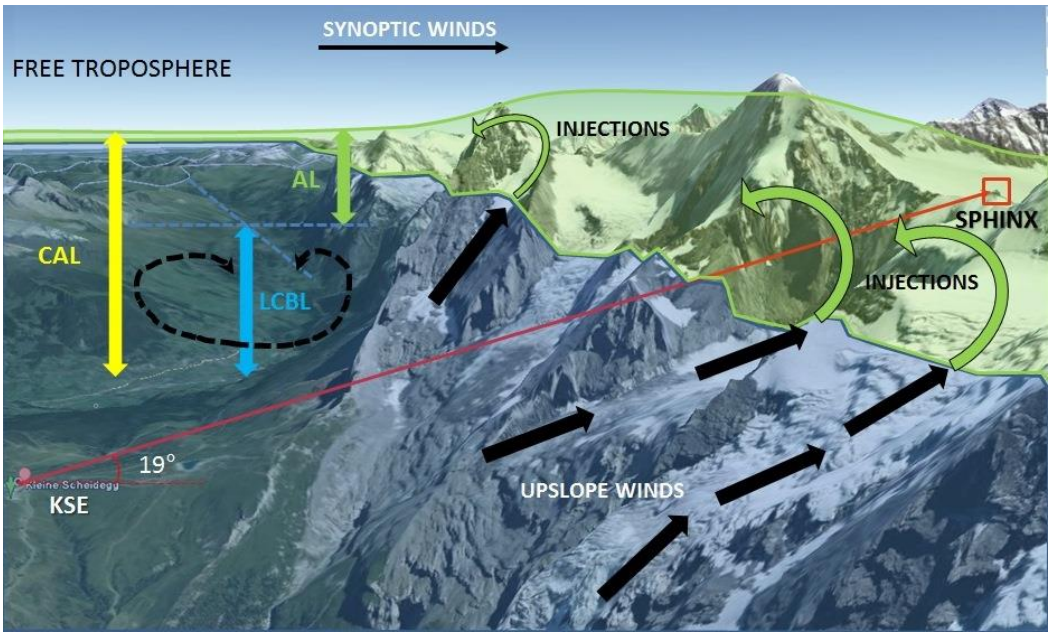

Figure 5. Schematic view of the daytime atmospheric structure and vertical pollution transport in and above the KSE site. The red line shows the CHM15k line of sight towards the Sphinx. The annotations denote the different thermal transport and mixing mechanisms of boundary layer air.

~~6.1.1 Annual cycle of the transport of CBL and CAL air masses to the JFJ~~

At the JFJ, aerosols and gases have been ~~sampled~~measured continuously since many years. Different sources and transport regimes towards the JFJ have been studied by many authors (e.g., Lugauer et al., 1998; Zellweger et al. 2003, Balzani Lööv et al. 2008, Henne et al. 2010, Collaud Coen et al., 2011; Collaud Coen et al., 2014; Herrmann et al. 2015) ~~and revealed~~showing that the JFJ resides ~~mostly~~most of the time in the undisturbed ("clean") lower FT~~, but that,~~. Nevertheless and especially in summer, ~~it~~the JFJ is influenced by thermally-induced ~~lifting of~~uplifted CBL air ~~and in general~~, it is also influenced by additional ~~vertical~~ lifting processes such as frontal passages and Föhn flows (Zellweger et al., 2003, Ketterer et al., 2014). ~~The frequently occurring (~35 % of the time)~~As observed by Zellweger et al. (2003) the thermally-induced transport of CBL air towards the JFJ ~~observed by Zellweger et al. (2003)~~ occurs frequently during summer ~~merits a closer look. In this sense, we want to provide a statistical description of the mechanisms leading the air to be thermally injected above the actual CBL and to reach the JFJ. Based on all these~~(~35 % of the time). The previous studies~~, it appears in fact~~ suggest that the direct contact of ~~the~~ undiluted ~~CBL~~LCBL air with the in-situ instruments at the JFJ occurs only rarely and is limited to ~~the~~ summer ~~period~~periods (e.g., Ketterer et al., 2014).

~~In the study by~~ Lugauer et al., (1998~~), the authors~~) provide a 9-year climatological analysis of the vertical transport of aerosols to the JFJ and the corresponding synoptic conditions. The thermally-induced transport is

Formatted: Font color: Black

nearly absent in winter or under cyclonic conditions and it is strongest in summer under anticyclonic periods. During favourable conditions, the aerosol concentration increases at the JFJ during the afternoon with a peak at around 18:00 UT and the peak is stronger in northern synoptic wind than in southern because of the difference in upwind topography. Collaud Coen et al. (2011) found as well that the JFJ is mainly influenced by free tropospheric air masses in winter and largely influenced by the LCBL (also during the night) in summer during subsidence periods.

In order to understand the impact of the thermally-driven dynamics on the in-situ measurements at the JFJ and ~~in the attempt~~ to quantify, by direct observations, the number of times that the LCBL and the CAL reach the JFJ throughout the year, the data from the CHM15k have been analysed using PathfinderTURB during the period August 2014 till November 2015.

~~6.2 Adaptation of~~ PathfinderTURB ~~in tilted configuration~~

~~A~~ has been adapted to use the CHM15k data along the slant-probing ~~version of the~~direction connecting KSE with JFJ. The adapted PathfinderTURB ~~algorithm that~~ version does not use the ~~atmospheric variance~~ $VAR(S)$ profiles to calculate the weights (eq. (~~2~~3)), but solely to retrieve the first transition to the enhanced turbulence zone (~~*liminf*), runs operationally on the KSE ceilometer since September 2014. The reason why, contrary to what happens~~see Sect. S2 in the Supplement). In fact, at ~~PAY, PathfinderTURB does not use the signal variance when calculating the weights to determine the geodesic path at KSE, depends entirely on the tilted configuration of the ceilometer. Altitudes higher than 1000 m a.g.l. correspond already to ranges farther than 3000 m along the laser's line of sight. At KSE, the backscatter signal at these ranges is often characterized by very little aerosol concentration, and is contaminated by significant contribution from the solar background. The backscatter signal is then dominated by the noise with low SNR and the calculated variance is not reliable. At closer~~close ranges, where the first transition to ~~turbulence~~the turbulent region is usually ~~to be~~ found, the ~~signal~~S profile has a much higher SNR and ~~the variance~~ $VAR(S)$ can be measured reliably. At KSE, the LCBL height (LCBLH) retrieved by PathfinderTURB, corresponds to the first discontinuity in the vertical mixing of aerosols and can be estimated also during nighttime.

~~6.3~~6.1 Retrieval of aerosol layers at KSE and JFJ

~~Installed at KSE at 2069 m a.s.l.,~~The CHM15k detects the ~~ceilometer can exclusively detect the aerosol layers~~ aerosols that form in the surrounding lower-altitude valleys (e.g., 1034 m a.s.l. Grindelwald, 566 m a.s.l. Interlaken) and that ~~reach higher than the altitude~~are transported above the KSE. Local generation of ~~KSE. As an exception~~ aerosols occurs only sparingly due to the reduced vegetation and the long periods of snow and ice cover. Nevertheless, when local ~~sources of aerosols may form a~~aerosols production occurs, these can be transported through the ceilometer's field of view and eventually be transported up to the JFJ. The local ~~aerosol layer that becomes visible to the ceilometer and that is independent~~aerosols generation and the advection from the ~~contribution of other aerosols from the adjacent valleys. These dynamics are valid during both day and night, but~~ surrounding valleys lead to different scenarios~~:~~. During daytime, both TCAL and LCBLH can be detected ~~during daytime at KSE~~, the LCBLH only during periods when ~~convection lift~~ the LCBL air is lifted into the

Formatted: Font: Arial

Formatted: Font: Arial, Font color: Auto

Formatted: Space Before: 0 pt

Formatted: Font color: Black, Engli (U.S.)

Formatted: Font color: Black

ceilometer's field of view~~; during~~ by convection. During nighttime, when there is no convection, only the TCAL can be detected (if it is present). ~~Likewise for any aerosol layers observed by the ceilometer above KSE, also the observed~~The nocturnal TCAL can ~~form~~stem from the residual layer ~~of~~formed above the surrounding valleys ~~(at least partially). Because~~. PathfinderTURB is based on the same retrieval principle during day and night, ~~i.e.~~and so it looks for the first discontinuity in the ~~well-mixed~~uninterrupted aerosol region~~,~~. For this reason and for simplicity we will refer to the retrieved ~~nighttime~~nocturnal boundary layer ~~also~~ as to ~~*mixing layer* or~~ LCBL even when the mixing is not due to convection, but rather to mechanical mixing from the surface and katabatic winds.

~~6.3.1~~6.1.1 LCBLH retrieval

The seasonal-averaged daily cycles of the retrieved LCBLH and TCAL during spring, summer ~~and~~, autumn and winter are shown in Figure 6. ~~During winter, (December 2014, January and February 2015) the algorithm has retrieved only a negligible number of LCBL heights and they have not been taken into account due to their lack of statistical significance.~~

During spring (~~Fig.~~Figure 6a), summer (~~Fig.~~Figure 6b) and (partially) autumn (~~Fig.~~Figure 6c), the LCBLH grows through morning till reaching a peak in the afternoon. In summer, the LCBLH has been retrieved by PathfinderTURB every day with only few exceptions. In Spring, (March-May), and in summer (June-August) the LCBL has reached the JFJ during 20 and 9 individual days, respectively. These occurrences lay above the 75 percentile of the LCBLH dataset and, hence, are not represented by the blue-shaded area in Figure 6a-b. From the systematic visual inspection and comparison of LCBLH ~~timeseries~~time series at PAY and KSE, we can say that the LCBLH peak occurs later at KSE than at ~~the~~ PAY. During the night, the LCBLH ~~decreases~~drops, due to the concurrent effects of aerosol gravitational settling, subsidence and katabatic ~~drainage flows~~winds, which result from radiative cooling of the surface triggering katabatic drainage flows. A likely explanation of the delay in the onset of the LCBL and of the afternoon peak at KSE is ~~the following:~~that due to the nighttime katabatic winds~~,~~ driving FT air ~~is driven~~ down into the valley~~. These katabatic~~ underneath. Depending on the season, these winds ~~also~~can continue to blow for ~~one or more~~few hours~~, depending on the season,~~ after sunrise (especially from the shaded mountain side) and work against the formation of the LCBL. The LCBLH temporal evolution follows the classical shape of a growing convective boundary layer like over flat terrain, but the growth and the duration of the LCBL occur over a shorter period. This is consistent with the delayed onset of the LCBL due to the persisting katabatic winds in the first hours of the morning and the earlier weakening of convection due to the shading effect of the surrounding mountains and the afternoon onset of the katabatic winds. This phenomenon is particularly enhanced during winter when the solar irradiance is at its minimum and the katabatic winds tend to suppress LCBL during most of the time.

~~Generally, the~~In autumn (September-November), the LCBLH shows a less pronounced daily cycle than in spring and summer, this is probably due to the fact that the vertical transport of aerosol-rich air is reduced by the stabilization within the lower troposphere during this period (Lugauer et al., 1998). ~~In summer, the LCBLH has been retrieved by PathfinderTURB every day with only few exceptions; from May to August the LCBLH retrievals have reached in the JFJ during short periods on 25 individual days , but these occurrences lay above the 75 percentile of the LCBLH dataset and, hence, are not represented by the blue shaded area in Fig.6.~~

In winter, (December-February) PathfinderTURB could retrieve only few LCBLH because of the very stable meteorological conditions, the reduced convection and the prolonged snow and ice cover limiting the aerosol production at KSE and the surrounding valleys. For this reason the seasonal-averaged daily cycle in Figure 6d does not show any particular pattern of the LCBLH, mainly due to the very low retrieval counts.

All occurrences of when the LCBLH and TCAL have reached the JFJ during the different months are listed in ~~the Table 1 and are shown in Figure 7 for winter and summer.~~ Table 1. ~~The LCBLH temporal evolution follows the classical shape of a growing convective boundary layer like over flat terrain, but the growth and the duration of the LCBL occur over a shorter period. This is consistent with the delayed onset of the LCBL due to the katabatic winds and the earlier weakening of convection under the contrasting action of the afternoon onset of the katabatic winds.~~

~~6.3.2~~6.1.2 TCAL retrieval

During spring and autumn, the daytime TCAL evolution is correlated with the LCBLH especially in spring during the first hours after sunrise (convective growth) and until the afternoon peak. The nighttime evolution of the TCAL in spring and autumn also shows a correlation ~~with the LCBLH,~~ although weaker, with the LCBLH. In summer, the TCAL does not show any significant correlation with the temporal evolution of the LCBLH ~~neither during the day nor during the night~~during day or night. During winter, the TCAL shows no correlation with the LCBLH. Despite an overall absence of a daily pattern of the winter LCBLH, the TCAL shows a clear outline during the period 00-10 UTC. This bimodal pattern with higher TCAL during the first part of the day could be explained by the process of dissipation of the CAL caused by the wind shear along the line of sight connecting KSE and JFJ when the solar irradiance modifies the wind dynamics during the central hours of the day.

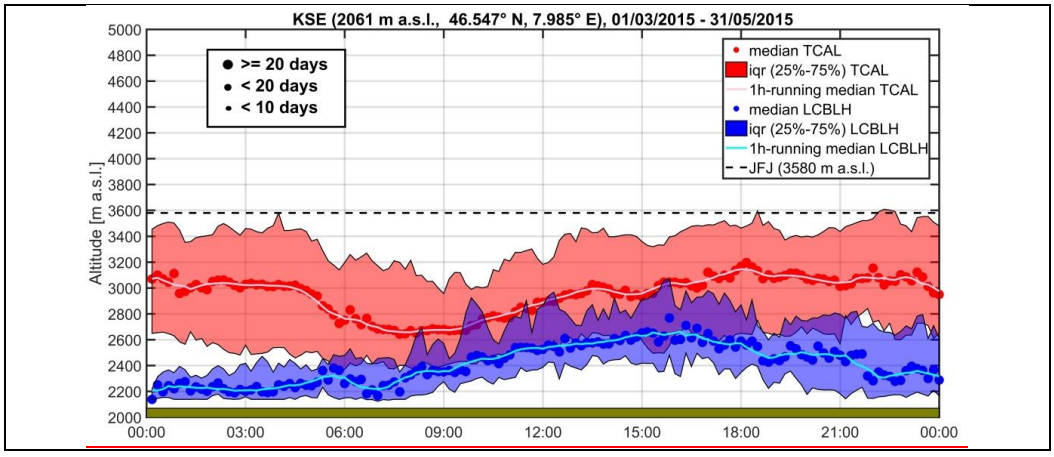

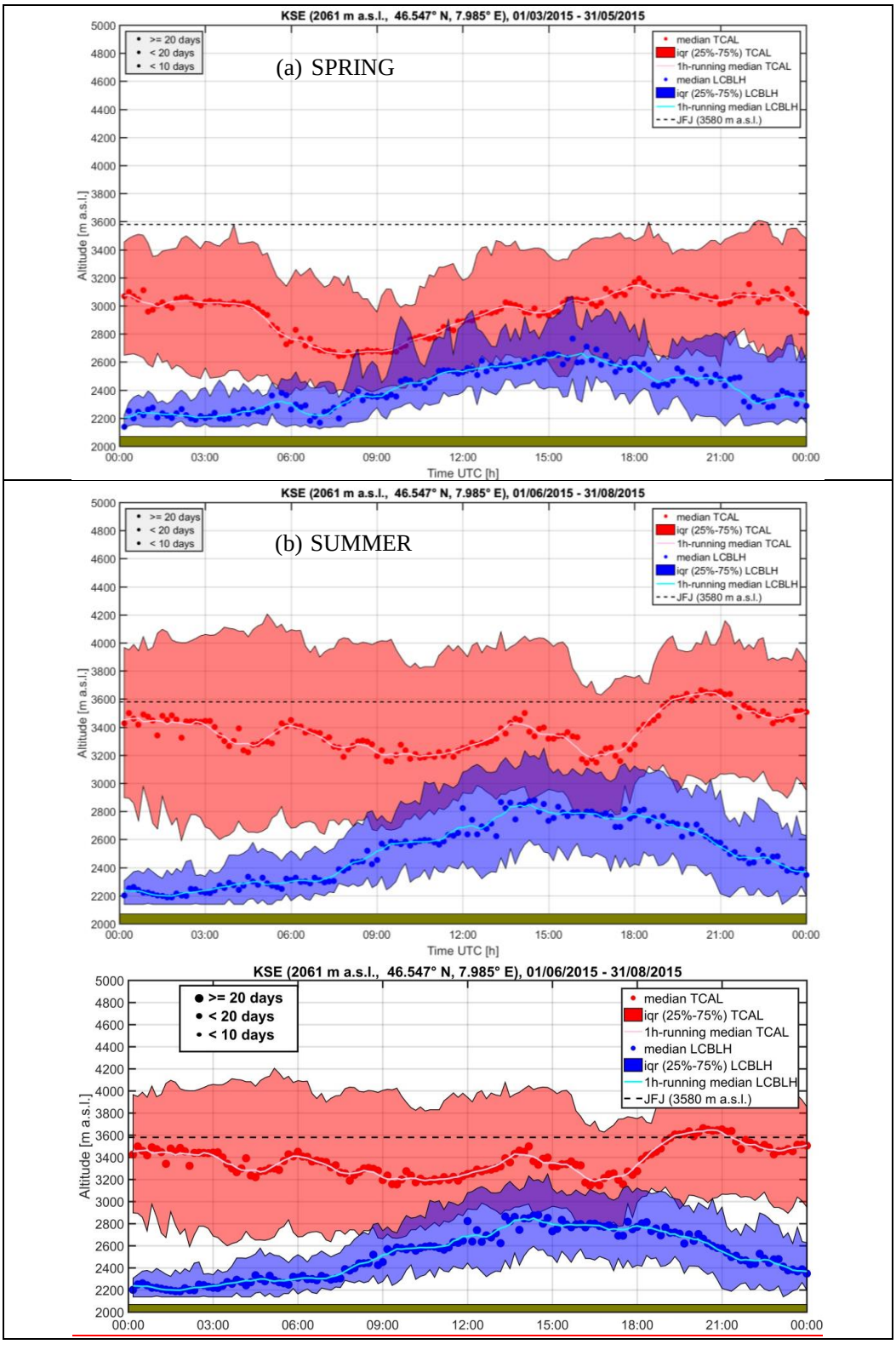
KSE (2061 m a.s.l., 46.547° N, 7.985° E), 01/03/2015 - 31/05/2015
(a) SPRING
>= 20 days
< 20 days
< 10 days
median TCAL
iqr (25%-75%) TCAL
1h-running median TCAL
median LCBLH
iqr (25%-75%) LCBLH
1h-running median LCBLH
JFJ (3580 m a.s.l.)
Altitude [m a.s.l.]
Time UTC [h]
KSE (2061 m a.s.l., 46.547° N, 7.985° E), 01/06/2015 - 31/08/2015
(b) SUMMER
>= 20 days
< 20 days
< 10 days
median TCAL
iqr (25%-75%) TCAL
1h-running median TCAL
median LCBLH
iqr (25%-75%) LCBLH
1h-running median LCBLH
JFJ (3580 m a.s.l.)
Altitude [m a.s.l.]
Time UTC [h]
KSE (2061 m a.s.l., 46.547° N, 7.985° E), 01/06/2015 - 31/08/2015
>= 20 days
< 20 days
< 10 days
median TCAL
iqr (25%-75%) TCAL
1h-running median TCAL
median LCBLH
iqr (25%-75%) LCBLH
1h-running median LCBLH
JFJ (3580 m a.s.l.)
Altitude [m a.s.l.]

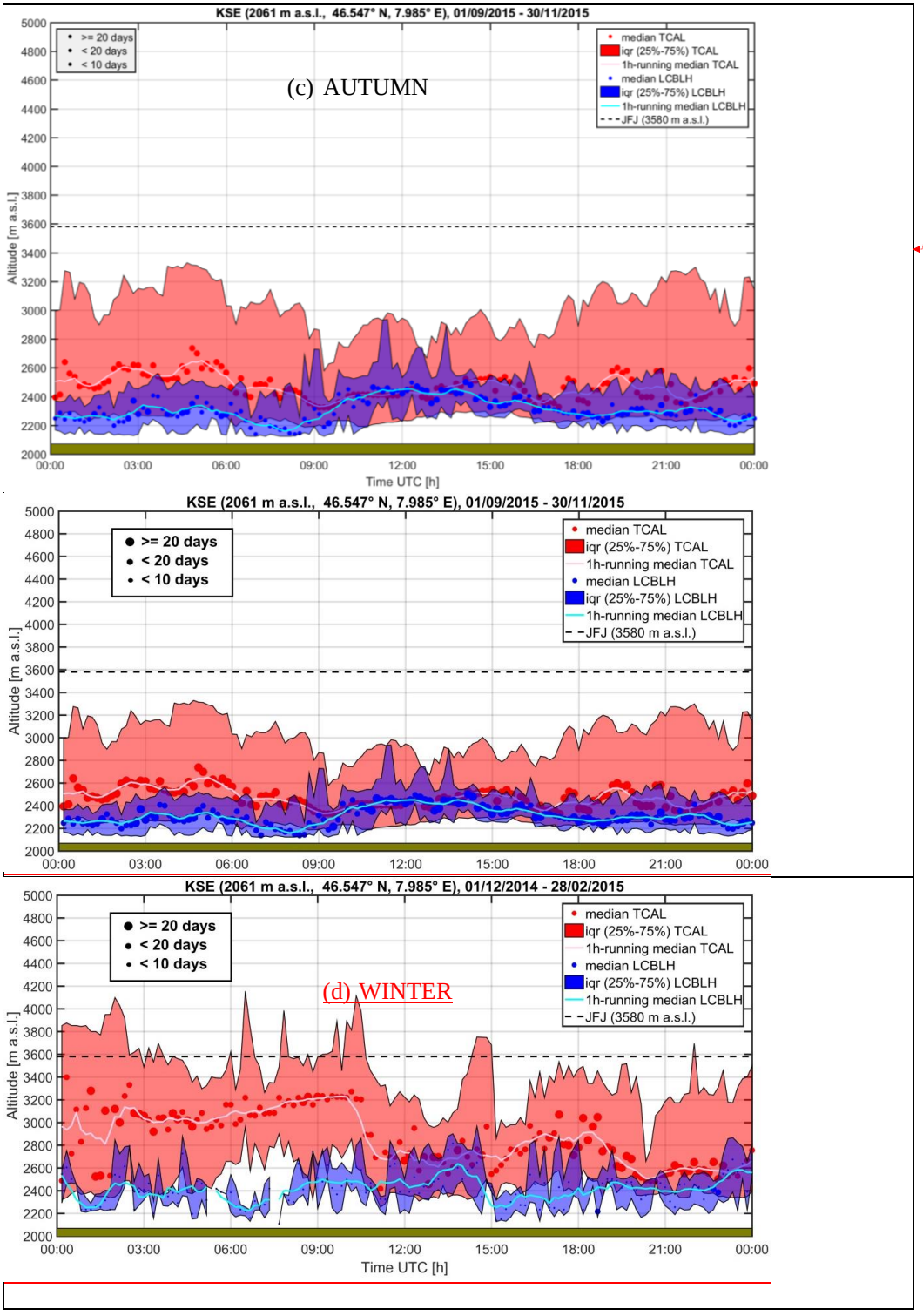

Formatted: Justified

Figure 6. Season-averaged daily cycle of the TCAL (red dots) and of the LCBLH (blue dots) at KSE. The size of the dots corresponds to the number of measurements available in each temporal bin. Panel a) ~~Spring~~spring (March to May~~). Panel~~); panel b) ~~Summer~~summer (June to August~~). Panel~~); panel c) ~~Autumn~~autumn (September to November~~)..~~); panel d) winter (January to February). Shaded areas show the 25%-75% inter-quartile range (iqr) for LCBL (purple) and TCAL (red). The altitude of JFJ is indicated by the black-dashed horizontal line.

~~As it will become clear in the next section, the CAL has a major impact on the aerosol measurements at JFJ, especially in summer. On the other hand, there is also a relationship between aerosol parameters observed at JFJ and LCBLH during the entire day.~~

~~6.3.3~~6.1.3 Occurrence frequency of LCBL and CAL reaching JFJ

~~In~~ Table 1 ~~we show~~shows, for each month during the studied period, the number of hours (cumulative 2-minute data points over the month), the number of days (number of days with at least one data point), and the percentage of time (time when the JFJ was inside LCBL or CAL as a percentage of the total time when the retrievals existed). On the left-hand side of the table, we show the statistics corresponding to when the JFJ is reached by or embedded into the LCBL, on the right-hand side we show the statistics corresponding to when the JFJ is either into the LCBL or the CAL (LCBL + AL). ~~The statistics reported in Table 1 are shown in the Circle charts in Figure 7, specifically for the winter (December-February) and summer (June-August) seasons.~~ The statistics show that during winter (light grey rows in Table 1) the aerosol measurements at the JFJ are never ~~modified~~ directly influenced by the LCBL air, which remains constantly below the JFJ. Moreover, the total duration of time when ~~the~~ PathfinderTURB has detected ~~a~~the LCBL rising above KSE (but not touching the JFJ) during winter accounts for no more than 65.52 hours. On the other hand, the CAL reaches the JFJ about one fourth of the time (21.23~~%) corresponding~~%), which corresponds to a duration of 109.44 hours (distributed over 26 days). The remaining three quarters of time (78.77%), corresponding to a duration of 406.32 hours, the JFJ is situated in the FT, i.e. the in-situ measurements are characterized by background (molecular) conditions. Although it is impossible to establish the exact origin of the air in the AL (i.e., the injection layer), we can speculate that winter AL is composed of aerosols originating from long-range transport and synoptic-scale lifting, rather than LCBL injections.

During summer (dark grey rows in Table 1) the situation changes significantly with the LCBL reaching the JFJ during the 3.63% of time, corresponding to 34.56 hours (distributed over 20 days).

Table 1: statistics of frequency of LCBL and CAL reaching or embedding the JFJ.

JFJ inside LCBL				**JFJ inside CAL**			
Date	**Hours**	**Days**	**%**	**Date**	**Hours**	**Days**	**%**
09/2014	4.87	2	1.94	09/2014	149.03	18	23.882
10/2014	8.00	4	5.81	10/2014	88.70	18	16.29
11/2014	1.67	3	4.20	11/2014	72.23	13	24.49

12/2014	0.00	0	0.00	12/2014	43.30	9	26.67
01/2015	0.00	0	0.00	01/2015	33.53	10	21.76
02/2015	0.00	0	0.00	02/2015	32.70	7	16.41
03/2015	0.2	1	0.12	03/2015	45.77	13	10.24
04/2015	5.67	3	3.59	04/2015	80.73	15	14.82
05/2015	5.43	5	2.21	05/2015	114.07	17	22.83
06/2015	0.50	2	0.16	06/2015	174.60	24	29.30
07/2015	18.60	12	5.61	07/2015	380.47	28	56.49
08/2015	15.50	6	5.17	08/2015	217.63	19	36.34
09/2015	0.97	2	0.51	09/2015	56.30	12	11.50
10/2015	0.00	0	0.00	10/2015	19.87	6	5.53
11/2015	0.2	1	0.36	11/2015	4.10	2	1.42

Although the relatively low percentage may induce to think of a marginal effect, the striking parameter is that during summer the undiluted, ~~polluted~~aerosol-laden air of the LCBL is able to reach the JFJ (and potentially strongly affect the in-situ measurements of particles concentrations and of their optical properties) on 20 different days. With regard to the frequency and duration when the CAL has reached or embedded the JFJ, the statistics are even more remarkable with the 40.92% of the time or 772.8 hours distributed over 71 days. Also for the summer statistics, no quantitative conclusions can be drawn about the origin and type of the aerosols inside the AL. The aerosols could be locally emitted and injected into the AL or transported ~~from~~over regional ~~to~~or continental ~~scale sources~~scales and could have been formed secondarily in the AL (Bianchi et al., 2016). In any case, the convective conditions occurring frequently during the summer ~~hint at~~suggest a significant mixing of the LCBL air into the FT forming the AL. Also the measurements by the in-situ instrumentations at the JFJ show that the absorption coefficient (indirectly proportional to the black carbon concentration) is largest during the summer period ~~(Fig. 8).~~.

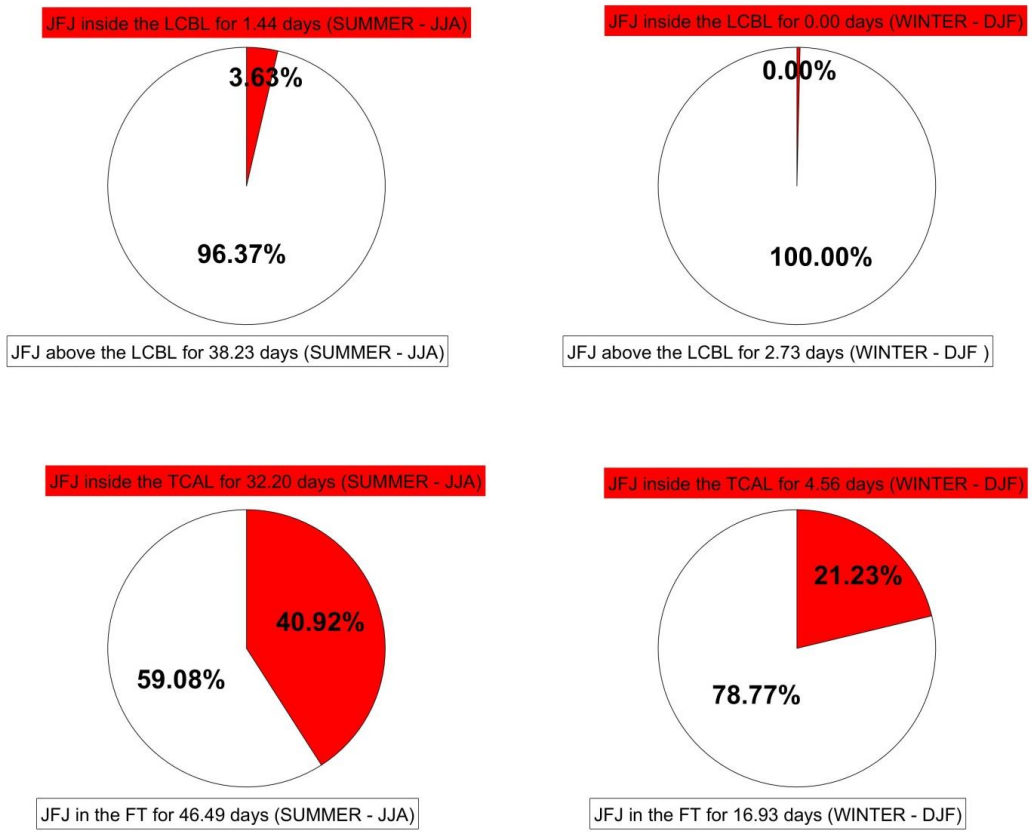

~~Figure 7. Circle chart of frequency of LCBL and CAL reaching or embedding the JFJ during summer (JJA) and winter (DJF). Red shaded areas show the percentage of time when the LCBL (CAL) is reaching or embedding the JFJ with respect to the total time when the retrievals exist. The white-shaded areas show the percentage of time when the JFJ sits inside the FT with respect to the total time when the retrievals exist.~~

As mentioned in the previous sections, these results are in agreement and confirm the indirect measurements and model simulations ~~of~~done in the previous works, especially those by Zellweger et al. (2003), Collaud Coen et al. (2011), Ketterer et al. (2014) and Herrmann et al. (2015). ~~In fact~~Here, and for the first time, the occurrence of the ~~frequency of the~~ convective (LCBL) and injection (AL) layers reaching directly the in-situ ~~measurements~~ instrumentation at the JFJ has been ~~quantitatively calculated thanks~~statistically analysed based on one year of data. The big advantage of applying PathfinderTURB to the ceilometer profiles is to have an automatic retrieval of the ~~two layers~~LCBLH and the TCAL directly at the JFJ. That allows to have real values of LCBLH or TCAL at the JFJ and not~~, like done~~ to use detections made in ~~the past, by extrapolated measurements of the boundary layer taken 5 km afar~~an atmosphere distant many kilometres from the JFJ~~ and based on~~. Moreover, not co-located measurements require stringent homogeneity conditions of the atmosphere between the point where the LCBLH and TCAL have been detected and the JFJ.

~~Next, we study the impact of the LCBL and the CAL on the JFJ measurement site by putting them in relation with the in-situ measurement of the absorption coefficient.~~

~~6.~~4~~6~~.2 Comparison with in-situ instrumentation

Figure 7 shows the relation ~~per season~~that exists between the ~~amplitude (max/min) of the diurnal cycles~~daily maximum of the LCBLH retrieved by ~~the~~ PathfinderTURB and the corresponding (in time) absorption coefficient, α, at 637 nm measured by the MAAP at the JFJ. ~~In the graph,~~The vertical red dashed line shows the altitude of the JFJ, each box collects all the ~~marker types account for~~LCBLH retrievals within 400-m of vertical span and the ~~fact that~~ corresponding values of α. In each box the ~~LCBL reaches (empty circles)~~number of LCBLH- α pairs is indicated by N and the ~~JFJ or not (filled circles).~~

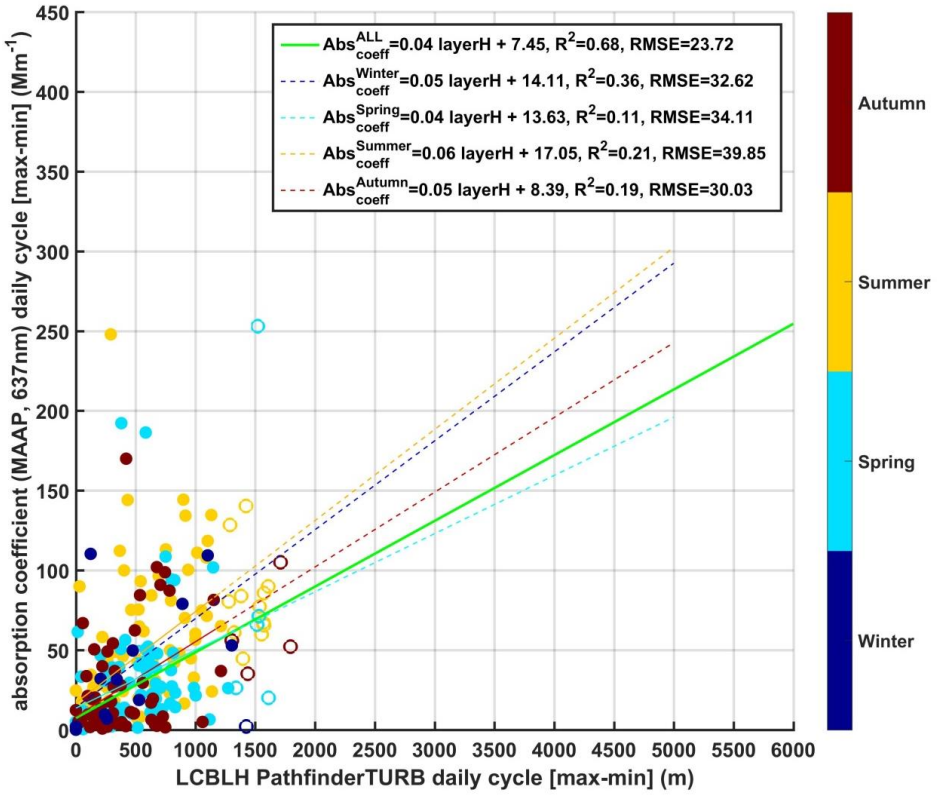

~~Figure 8 Scatter plot of~~ median of each box is connected by the ~~amplitude (max-min) of~~ black dashed line to show the ~~diurnal cycles of~~median trend. The data in the box-plot are from all seasons, in order to maximize the number of occurrences and increase the statistical significance of the trend.

Formatted: Font color: Black

Formatted: Font color: Black

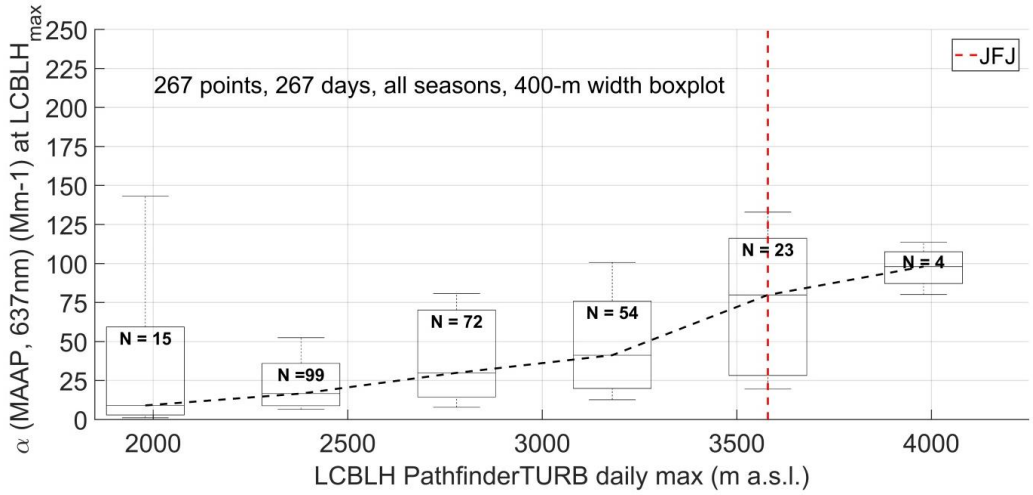

Figure 7. Box-plot showing the relation between the absorption coefficient at 637 nm measured by the MAAP at the JFJ vs the LCBLH retrieved by PathfinderTURB for the period September 2014 to November 2015.

~~A positive relation between LCBLH and absorption coefficient is thought to exist especially for times when the LCBL does not reach the JFJ (filled circles). In these situations, when the LCBL grows deeper and approaches the height of the JFJ, the injections of LCBL air into the AL are more likely to occur and bring more aerosols to the in-situ instruments. In this case the amplitude of the daily cycle of the absorption coefficient is greatest, as the difference between the convective peak of the LCBL (large injections) and its minimum (negligible injections) correspond to high and low absorption coefficients, respectively. On the contrary, when the LCBLH is higher than the JFJ for a few hours during the day, the residual AL is also richer in particles and the amplitude of the daily cycle of the absorption coefficient is much smaller (the absorption remains large all day). During summer and for LCBLH < JFJ (filled circles) convection causes significant injections into the AL leading to large amplitude of the daily cycle of the absorption coefficient (larger slope in Fig.8). On the other hand, during spring probably due to the thick layer of snow accumulated during winter, the convection is too weak to create significant injections into the AL, and relatively deep LCBL do not correspond to large daily cycles in the absorption (smaller slope). Despite the low coefficients of determination of the seasonal fits, when all points are fitted together the dependency of the max-min cycle of the absorption coefficient on the LCBLH becomes clearer.~~

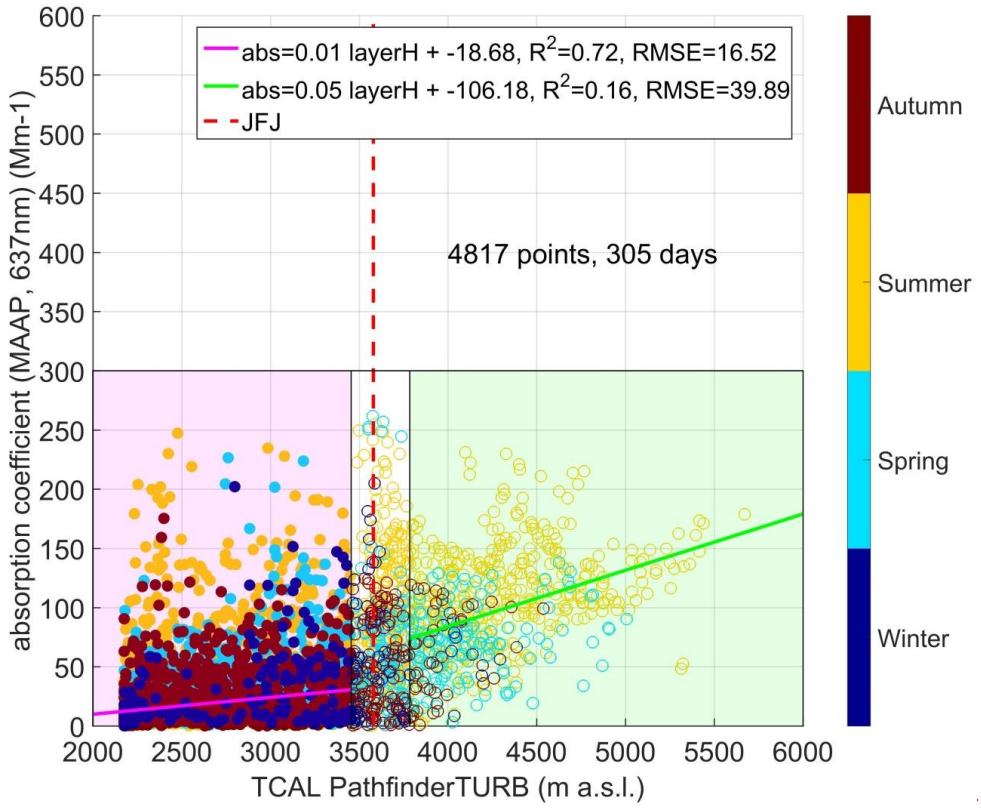

~~Figure 9 Scatter~~ A linear median trend characterised by a small slope could be fitted to the LCBLH-α pairs for LCBLH lower than the JFJ (2000-3380 m). For these range of altitudes the LCBL grows deeper getting closer to the height of the JFJ. The injections of LCBL air into the AL (embedding the JFJ) are then more likely to occur when the LCBLH reaches its maximum injecting LCBL air past the in-situ sensors with a resulting higher value of α. As soon as the LCBLH reaches the JFJ, the injections into the AL reaching the in-situ instrumentation become more important and this is shown by the change in slope of the median trend. When the LCBLH maxima are higher than the JFJ, the in-situ instrumentation are reached by undiluted, aerosol-laden LCBL air and the absorption coefficient α grows even more. In addition to the slope of the median trend, it is important to explain the interquartile variability of each box and their physical meaning. The first box centred at about 2000 m shows a large interquartile range of α values, this is due to Saharan dust events occurring mainly during Autumn and winter above the LCBLH and increasing significantly the value of α. The box centred at the JFJ height also shows a large interquartile range of α values, in this case the variability is due to the large α values corresponding to the LCBLH higher than the JFJ and the smaller α values corresponding to the LCBLH lower than the JFJ. In conclusion, Figure 7 shows clearly the impact of the LCBL air on the absorption coefficient α measured at the JFJ.

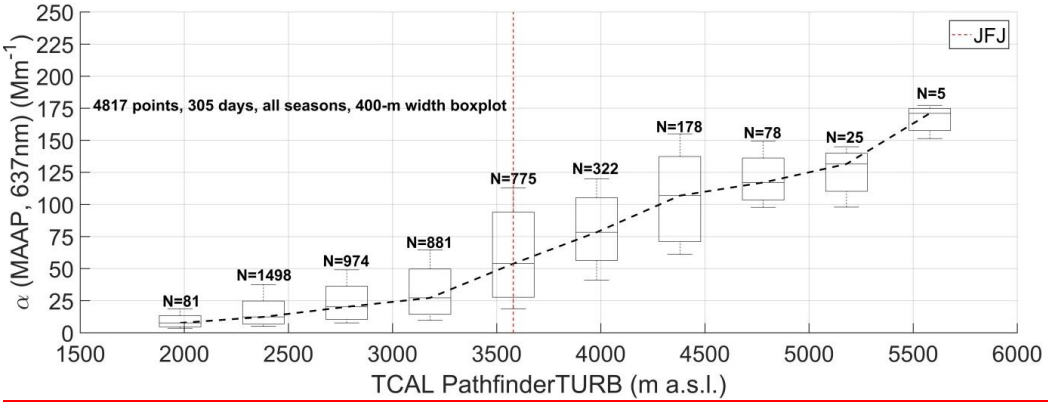

Figure 8. Box-plot ~~of~~showing the ~~height of the TCAL vs~~relation between the absorption coefficient at 637 nm measured by the MAAP at the JFJ ~~during~~vs the LCBLH retrieved by PathfinderTURB for the period September 2014 to November 2015. ~~Two independent linear regressions were fit to the data when TCAL was below (magenta line) and above (green line) the JFJ.~~

~~The~~ In the same way as in Figure 7 for the LCBLH, Figure 8 shows the relation between ~~the TCAL~~α and the ~~absorption coefficient at 637 nm,~~TCAL. Differently from Figure 7, not only the maxima of α and TCAL are shown in ~~Figure 9, has been studied in a slightly different way than for~~ the ~~LCBLH case~~box-plot, but all the hourly data from all seasons. The TCAL represents the upper boundary of the AL ~~or of the LCBL (when the AL is not present),~~, when the TCAL is below the JFJ ~~(TCAL < JFJ)~~ the in-situ instrumentation on the JFJ is located inside the FT showing very little absorption ~~and a negligible daily cycle of the absorption. When the TCAL reaches or embeds the JFJ (TCAL > JFJ) the absorption grows~~. Within the range of altitudes 2000-3380 m, the slope of the median trend is smaller than the one in Figure 7, this is because even when the TCAL grows deeper towards the JFJ, the strength of the injections coming from beneath the AL is insufficient to influence significantly the absorption measurements. As for the LCBL, also for the TCAL when it reaches the JFJ the α values become larger and the slope changes accordingly. Because the aerosols injected into the AL do not undergo a convective mixing, they tend to settle under the gravity force leading to higher aerosol concentration at the bottom than at the top of the AL. Also for this reason the absorption grows larger accordingly to a higher TCAL~~. Instead of the daily cycle of the absorption coefficient, Figure 9 shows, the hourly values of absorption versus the hourly TCAL values. The relation is shown in Figure 9 separately for TCAL < JFJ (filled circles) and TCAL > JFJ (empty circles). In each region, the data have been linearly fitted. As expected, for the region TCAL < JFJ the absorption coefficient does not depend (or only negligibly) on the TCAL. The absorption remains very low during all seasons except for summer when sporadic injections manage to push aerosols higher above the detected TCAL. In the region TCAL > JFJ, as the CAL grows beyond the altitude of JFJ, the absorption coefficient shows a linear dependence on the depth of the CAL. Data points, when TCAL was within the central region that spans 330 m around the JFJ's station height (3580 m), were omitted from the regression in order to more clearly separate between representative FT and AL conditions.~~ (3380-4580 m) and the slope of the trend remain almost constant showing the linearity of the physical process. For higher altitudes (z > 4580 m) α continues to grow, but at a lower rate and with a decreasing number of occurrences. Also for the TCAL- α

Formatted: Line spacing: 1.5 lines

relation the interquartile range of the box centred at the height of the JFJ is larger than the other boxes showing larger values of α for TCAL > JFJ and smaller α for TCAL < JFJ.

In order to summarizing the results shown in Figures 7 and 8, we provide in Figure 9 the overall impact of the LCBL, CAL and FT on the in-situ measurements of α. Each box collects all data from all seasons corresponding to the background atmosphere (FT), the partially mixed air (CAL) and the undiluted, aerosol-laden air (LCBL) with respect to the position of the JFJ. This box-plot represents perfectly the impact of the three atmospheric regions and confirms the importance of an automatic monitoring of the atmosphere at the JFJ and in general in the mountainous regions where the dynamics are complex due to topography and wind circulation.

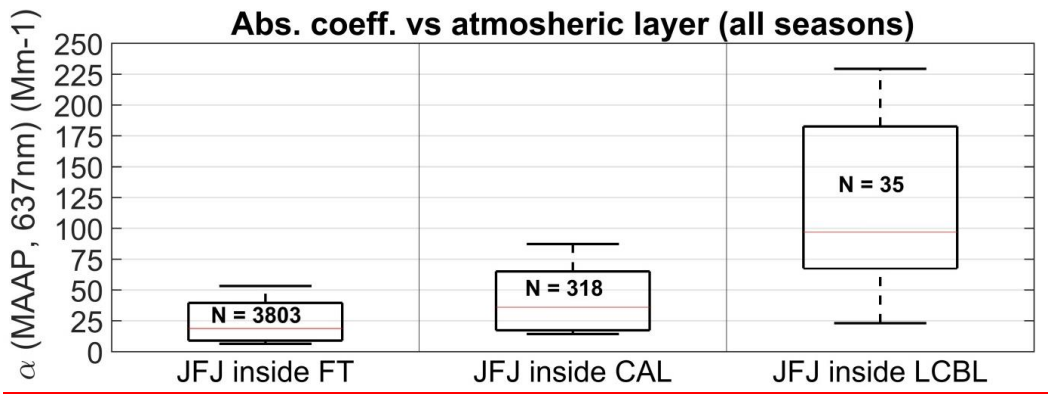

Figure 9. Box-plot of α and FT, CAL, LCBL pairs. Each portion collects all pairs over the corresponding atmospheric region for all seasons.

7 Conclusions

A novel algorithm, PathfinderTURB, has been developed, validated and applied to ~~the real-time retrieval of~~retrieve the vertical structure of the planetary boundary layer. ~~Its main advantages can be summarized as it follows.~~ PathfinderTURB provides reliable estimates of the daytime convective boundary layer height (CBLH) and of the Top of the Continuous Aerosol Layer (TCAL~~). The retrieval of the two layers is performed~~) operationally and without need of ancillary data or any a priori information (except for climatological limits) from a model. PathfinderTURB can also be adapted to different probing line's angles and types of instrument. For this study, two settings have been ~~especially~~ tested and applied to the data of ~~a~~two CHM15k, the vertical-pointing and tilted-pointing~~, but PathfinderTURB can be easily adapted to any other angles and types of ceilometer. In perspective, based on the adaptability of the algorithm to diverse topographic conditions and on the fact that it does not require real-time ancillary data, PathfinderTURB is best suited to treat a large dataset from networks of ceilometers in real time.~~.

~~PathfinderTURB suffers anyway some limitations related to the instrument. Due to the incomplete transmitter-receiver overlap in the first few hundred meters, and the unphysical gradients occurring in this zone, PathfinderTURB, which is partly gradient-based, is affected by a larger uncertainty in the first few hundred meters. Another limitation is that during the late afternoon, the aerosols remain suspended in the air (transition from CBL to RL) showing no detectable aerosol gradient at the top of the CBL. The only detectable gradient~~

~~remains normally at the same altitude as the maximum CBL height reached during the central hours of the day, and corresponds more to the RL top rather than to the decaying CBL top. In fact, any method using aerosols as tracers (e.g. LIDAR) is not best suited to detect the afternoon CBL drop, but rather the RL.~~

~~The algorithm~~PathfinderTURB has been applied to one year of data measured by two CHM15k ceilometers operated at the Aerological Observatory of Payerne, on the Swiss Plateau, and at the Kleine Scheidegg, in the Swiss Alps. The algorithm has been ~~first~~ thoroughly evaluated and validated at ~~the~~ Payerne ~~station. At Payerne, the~~. The CBLH retrievals obtained by PathfinderTURB have been compared ~~with~~against two references, (i) the manual detections by human experts ~~that acted as reference for the CBLH values and with~~and (ii) the noon CBLH values retrieved by two methods based on ~~the thermal structure of the atmosphere and using the~~ radiosounding data: the parcel method and the bulk Richardson method. ~~The comparison against the human experts reference revealed a median difference of 27 m and a RMSE of 76 m. The median difference with respect to the radiosounding reference is 53 m with a RMSE of 162 m.~~

Based on the excellent agreement with the two ~~reference methods, the~~references, PathfinderTURB has been applied to the ~~complex terrain site at the~~ ceilometer's backscatter profiles between the Kleine Scheidegg and the Jungfraujoch (JFJ) for the period September 2014-November 2015. ~~There,~~ The real-time monitoring of the local CBL (LCBL) ~~is retrieved based on the data of the CHM15k whose axis has been tilted by a zenith angle of 71° in order to probe the air volume next to the Sphinx Observatory (3580 m, a.s.l.) on the Jungfraujoch.~~

~~The results presented in Section 6 showed that the PathfinderTURB can be adapted to slant-path probing, thus providing real time and continuous LCBLH and~~ and the TCAL ~~data along the line of sight of the CHM15k. This~~ at the JFJ has allowed to ~~separate~~quantify the ~~contribution~~occurrence of these two layers and to understand their impact on the absorption coefficient, α, measured in-situ at JFJ.

~~The season-averaged daily cycle shows~~ The results have shown that the CAL reaches or includes the JFJ ~~for~~during the 40.92% of the ~~total~~ time in summer and ~~for~~ the 21.23% ~~of the total time~~ in winter for a total of 97 days during the two seasons. ~~The statistics suggest that the CAL modifies the physical and chemical properties of the air sampled at JFJ, especially during summer when the absorption coefficient at 637 nm at JFJ shows a distinct dependence on the CAL depth.~~

~~The season-averaged daily cycles show that the~~The LCBL reaches or includes the JFJ for short periods (3.94% of the ~~total~~ time) on 20 days in summer and never during winter. The ~~statistics suggest that also~~impact of the LCBL ~~modifies the physical and chemical properties of the air sampled at JFJ, but exclusively during summer, as these~~and CAL on the in-situ measurements ~~refer purely to the direct contact of undiluted~~of α at the JFJ is unambiguously shown in Figures 7 and 8 for different ranges of altitudes. The relation of the LCBLH- α and TCAL- α pairs is linear, but with different slopes for altitudes below and above the JFJ, with a clear modification of α due to the injections of the LCBL air ~~with the JFJ. During summer the amplitude of the daily cycle of the absorption coefficient at 637 nm reveals that the amplitude is largest when the LCBLH approaches~~ into the aerosol layer (AL) reaching the in-situ instrumentation at the JFJ ~~and starts levelling when the LCBLH exceeds the JFJ.~~

~~As~~. In a more general ~~conclusion, we can state that the~~ way, the overall impact of the LCBL, CAL and FT on the in-situ measurements of α is shown in figure 9. As expected the LCBL modifies more the in-situ measurements

at the JFJ in terms of absolute value of α, but it is outnumbered by a factor of 10 in terms of occurrences by the CAL. The CAL is in fact more diluted than the LCBL but embeds the JFJ 10 times more frequently than the LCBL and then its impact on the in-situ measurements is significant. The rest of the time the JFJ is within the FT with values of absorption characteristic of a molecular atmosphere.

The results obtained at ~~the~~ KSE ~~site~~and JFJ, are in agreement and confirm the indirect measurements and model simulations of previous works, especially those by Zellweger et al. (2003), Collaud Coen et al. (2011), Ketterer et al. (2014) and Herrmann et al. (2015). ~~In fact for the first time the impact of the convective (LCBL) and injection (AL) layers on the in-situ measurements at JFJ has been quantitatively calculated for a complete year thanks to the automatic retrieval of the two layers directly at the JFJ.~~Differently from the previous, our study has provided for the first time the possibility to calculate the occurrences of the convective (LCBL) and injection (AL) layers directly at the JFJ. The added value is the real-time application of PathfinderTURB to the ceilometer profiles connecting KSE to the JFJ and the possibility to have automatic LCBLH and the TCAL values at the JFJ. Indeed, before our study, LIDARs, ceilometers and wind profilers have always been used for vertical probing at a fixed distance (5-15 km) from the JFJ, which required stringent assumptions about the homogeneity of the atmosphere between the measurement site and the JFJ. The results presented have proven the importance of an automatic monitoring of the atmosphere at the JFJ and in general in the mountainous regions where the dynamics are complex due to topography and wind circulation.

In perspective, based on the adaptability of PathfinderTURB to diverse topographic conditions and on the fact that it does not require real-time ancillary data, PathfinderTURB is best suited to treat a large dataset from networks of ceilometers in real time.

Acknowledgements

This study has been financially supported by the SNF through ICOS-CH. The authors would further like to thank Nicolas Bukowiecki for giving access to JFJ aerosol measurement data. The authors are grateful to Kornelia Pönitz and Holger Wille (Lufft) for technical information about the CHM15k.

References

Angelini, F., Barnaba, F., Landi, T. C., Caporaso, L. and Gobbi, G. P.: Study of atmospheric aerosols and mixing layer by LIDAR, Radiat. Prot. Dosimetry, 137(3-4), 275–279, doi:10.1093/rpd/ncp219, 2009.

Baars, H., Ansmann, A., Engelmann, R. and Althausen, D.: Continuous monitoring of the boundary-layer top with lidar, Atmos. Chem. Phys., 8(23), 7281–7296, doi:10.5194/acp-8-7281-2008, 2008.

Balzani Lööv, J. M., S. Henne, G. Legreid, J. Staehelin, S. Reimann, A. S. H. Prévôt, M. Steinbacher, and M. K. Vollmer: Estimation of background concentrations of trace gases at the Swiss Alpine site Jungfraujoch (3580 m a.s.l.), J. Geophys. Res., 113, D22305, doi:10.1029/2007JD009751, 2008

Bianchi, F., Tröstl, J., Junninen, H., Frege, C., Henne, S., Hoyle, C. R., Molteni, U., Herrmann, E., Adamov, A., Bukowiecki, N., Chen, X., Duplissy, J., Gysel, M., Hutterli, M., Kangasluoma, J., Kontkanen, J., Kürten, A., Manninen, H. E., Münch, S., Peräkylä, O., Petäjä, T., Rondo, L., Williamson, C., Weingartner, E., Curtius, J.,

Worsnop, D. R., Kulmala, M., Dommen, J., and Baltensperger, U.: New particle formation in the free troposphere: A question of chemistry and timing, Science, 352, 1109-1112, doi: 10.1126/science.aad5456, 2016.

Biavati, G.: On the Retrieval of Mixing Height from Ceilometers, PhD thesis, Leipzig University, March 2014.

Brooks, I. M.: Finding Boundary Layer Top: Application of a Wavelet Covariance Transform to Lidar Backscatter Profiles, J. Atmos. Ocean. Technol., 20(8), 1092–1105, doi:10.1175/1520-0426(2003)020<1092:FBLTAO>2.0.CO;2, 2003.

de Bruine, M., Apituley, A., Donovan, D., Klein Baltink, K., and de Haij, M.: Pathfinder: Applying graph theory for consistent tracking of daytime mixed layer height with backscatter lidar, Atmos. Meas. Tech. Disc., 1-26, doi:10.5194/amt-2016-327,, 2016.

Bucholtz, A.: Rayleigh-scattering calculations for the terrestrial atmosphere, Appl. Opt., 34(15), 2765, doi:10.1364/AO.34.002765, 1995.

Bukowiecki, N., Weingartner, E., Gysel, M., Collaud Coen, M. C., Zieger, P., Herrmann, E., Steinbacher, M., Gäggeler, H. W. and Baltensperger, U.: A Review of More than 20 Years of Aerosol Observation at the High Altitude Research Station Jungfraujoch, Switzerland (3580 m a.s.l.), Aerosol Air Qual. Res., 16(3), 764–788, doi:10.4209/aaqr.2015.05.0305, 2016.

Canny, J.: A Computational Approach to Edge Detection, IEEE Trans. Pattern Anal. Mach. Intell., PAMI-8(6), 679–698, doi:10.1109/TPAMI.1986.4767851, 1986.

Cohn, S. A. and Angevine, W. M.: Boundary Layer Height and Entrainment Zone Thickness Measured by Lidars and Wind-Profiling Radars, J. Appl. Meteorol., 39(8), 1233–1247, doi:10.1175/1520-0450(2000)039<1233:BLHAEZ>2.0.CO;2, 2000.

Collaud Coen, M., Weingartner, E., Furger, M., Nyeki, S., Prévôt, A. S. H., Steinbacher, M. and Baltensperger, U.: Aerosol climatology and planetary boundary influence at the Jungfraujoch analyzed by synoptic weather types, Atmos. Chem. Phys., 11(12), 5931–5944, doi:10.5194/acp-11-5931-2011, 2011.

Collaud Coen, M., Praz, C., Haefele, A., Ruffieux, D., Kaufmann, P. and Calpini, B.: Determination and climatology of the planetary boundary layer height above the Swiss plateau by in situ and remote sensing measurements as well as by the COSMO-2 model, Atmos. Chem. Phys., 14(23), 13205–13221, doi:10.5194/acp-14-13205-2014, 2014.

Davis, K. J., Gamage, N., Hagelberg, C. R., Kiemle, C., Lenschow, D. H. and Sullivan, P. P.: An Objective Method for Deriving Atmospheric Structure from Airborne Lidar Observations, J. Atmos. Ocean. Technol., 17(11), 1455–1468, doi:10.1175/1520-0426(2000)017<1455:AOMFDA>2.0.CO;2, 2000.

Dijkstra, E. W.: A note on two problems in connexion with graphs, Numer. Math., 1(1), 269–271, doi:10.1007/BF01386390, 1959.

Engelbart, D., Reichardt, J. and Teschke, G.: Intercomparison of methods for determination of mixing heights using a new network of single-photon-counting high-sensitivity ceilometers in Germany, in TECO-2008 - WMO Technical Conference on Meteorological and Environmental Instruments and Methods of Observation. [online]

Available from: https://www.wmo.int/pages/prog/www/IMOP/publications/IOM-96_TECO-2008/P1(02)_Engelbart_Germany.pdf, 2008.

Flentje, H., Claude, H., Elste, T., Gilge, S., Köhler, U., Plass-Dülmer, C., Steinbrecht, W., Thomas, W., Werner, A. and Fricke, W.: The Eyjafjallajökull eruption in April 2010 – detection of volcanic plume using in-situ measurements, ozone sondes and lidar-ceilometer profiles, Atmos. Chem. Phys., 10(20), 10085–10092, doi:10.5194/acp-10-10085-2010, 2010.

Frey, S., Pönitz, K., Teschke, G. and Wille, H.: Detection of aerosol layers with ceilometers and the recognition of the mixed layer depth, in International Symposium for the Advancement of Boundary Layer Remote Sensing (ISARS). [online] Available from: http://www.isars2010.uvsq.fr/images/stories/PosterExtAbstracts/P_BLS12_Frey.pdf, 2010.

de Wekker, S. F. J.: Structure and morphology of the convective boundary layer in mountainous terrain, University of British Columbia, November., 2002.

Di Giuseppe, F., Riccio, A., Caporaso, L., Bonafé, G., Gobbi, G. P. and Angelini, F.: Automatic detection of atmospheric boundary layer height using ceilometer backscatter data assisted by a boundary layer model, Q. J. R. Meteorol. Soc., 138(664), 649–663, doi:10.1002/qj.964, 2012.

Haeffelin, M., Angelini, F., Morille, Y., Martucci, G., Frey, S., Gobbi, G. P., Lolli, S., O'Dowd, C. D., Sauvage, L., Xueref-Rémy, I., Wastine, B. and Feist, D. G.: Evaluation of Mixing-Height Retrievals from Automatic Profiling Lidars and Ceilometers in View of Future Integrated Networks in Europe, Boundary-Layer Meteorol., 143(1), 49–75, doi:10.1007/s10546-011-9643-z, 2012.

de Haij, M. J., Wauben, W. M. F., Baltink, H. K. and Apituley, A.: Determination of the mixing layer height by a ceilometer, in Proc. of the 8th International Symposium on Tropospheric Profiling. [online] Available from: http://www.knmi.nl/publications/fulltexts/rp_bsikinsa_knmi_20090729_paper_istp2009_dehaijetal_final_copy1.pdf, 2010.

Heese, B., Flentje, H., Althausen, D., Ansmann, A. and Frey, S.: Ceilometer lidar comparison: backscatter coefficient retrieval and signal-to-noise ratio determination, Atmos. Meas. Tech., 3(6), 1763–1770, doi:10.5194/amt-3-1763-2010, 2010.

Henne, S., Furger, M., Nyeki, S., Steinbacher, M., Neininger, B., de Wekker, S. F. J., Dommen, J., Spichtinger, N., Stohl, A. and Prévôt, A. S. H.: Quantification of topographic venting of boundary layer air to the free troposphere, Atmos. Chem. Phys., 4(2), 497–509, doi:10.5194/acp-4-497-2004, 2004.

Henne, S., D. Brunner, D. Folini, S. Solberg, J. Klausen, and B. Buchmann (2010), Assessment of parameters describing representativeness of air quality in-situ measurement sites, Atmos. Chem. Phys., 10, 3561–3581, doi:10.5194/acp-10-3561-2010.

Herrmann, E., et al.:Analysis of long-term aerosol size distribution data from Jungfraujoch with emphasis on free tropospheric conditions, cloud influence, and air mass transport, J. Geophys. Res. Atmos., 120, 9459–9480, doi:10.1002/2015JD023660, 2015

Hervo, M., Poltera, Y. and Haefele, A.: An empirical method to correct for temperature dependent variations in

the overlap function of CHM15k ceilometers, Atmos. Meas. Tech., 9, 2947-2959, doi:10.5194/amt-9-2947-2016, 2016.

Holzworth, G. C.: Estimates of mean maximum mixing depths in the contiguous United States, Mon. Weather Rev., 92(5), 235–242, 1964.

Hooper, W. P. and Eloranta, E. W.: Lidar Measurements of Wind in the Planetary Boundary Layer: The Method, Accuracy and Results from Joint Measurements with Radiosonde and Kytoon, J. Clim. Appl. Meteorol., 25(7), 990–1001, doi:10.1175/1520-0450(1986)025<0990:LMOWIT>2.0.CO;2, 1986.

Ketterer, C., Zieger, P., Bukowiecki, N., Collaud Coen, M., Maier, O., Ruffieux, D. and Weingartner, E.: Investigation of the Planetary Boundary Layer in the Swiss Alps Using Remote Sensing and In Situ Measurements, Boundary-Layer Meteorol., 151(2), 317–334, doi:10.1007/s10546-013-9897-8, 2014.

Lammert, A. and Bösenberg, J.: Determination of the convective boundary-layer height with laser remote sensing, Boundary-Layer Meteorol., 119(1), 159–170, doi:10.1007/s10546-005-9020-x, 2006.

Lenschow, D. H., Wulfmeyer, V. and Senff, C.: Measuring Second- through Fourth-Order Moments in Noisy Data, J. Atmos. Ocean. Technol., 17(10), 1330–1347, doi:10.1175/1520-0426(2000)017<1330:MSTFOM>2.0.CO;2, 2000.

Lugauer, M., Baltensperger, U., Furger, M., Gäggeler, H. W., Jost, D. T., Schwikowski, M. and Wanner, H.: Aerosol transport to the high Alpine sites Jungfraujoch (3454 m asl) and Colle Gnifetti (4452 m asl), Tellus B, 50(1), 76–92, doi:10.3402/tellusb.v50i1.16026, 1998.

Martucci, G., Matthey, R., Mitev, V. and Richner, H.: Comparison between Backscatter Lidar and Radiosonde Measurements of the Diurnal and Nocturnal Stratification in the Lower Troposphere, J. Atmos. Ocean. Technol., 24(7), 1231–1244, doi:10.1175/JTECH2036.1, 2007.

Martucci, G., Milroy, C. and O'Dowd, C. D.: Detection of Cloud-Base Height Using Jenoptik CHM15K and Vaisala CL31 Ceilometers, J. Atmos. Ocean. Technol., 27(2), 305–318, doi:10.1175/2009JTECHA1326.1, 2010a.

Martucci, G., Matthey, R., Mitev, V. and Richner, H.: Frequency of Boundary-Layer-Top Fluctuations in Convective and Stable Conditions Using Laser Remote Sensing, Boundary-Layer Meteorol., 135(2), 313–331, doi:10.1007/s10546-010-9474-3, 2010b.

Menut, L., Flamant, C., Pelon, J. and Flamant, P. H.: Urban boundary-layer height determination from lidar measurements over the Paris area, Appl. Opt., 38(6), 945–954, doi:10.1364/AO.38.000945, 1999.

Morille, Y. and Haeffelin, M.: Image processing to retrieve mixing layer depth with lidar, in International Symposium for the Advancement of Boundary Layer Remote Sensing (ISARS). [online] Available from: http://www.isars2010.uvsq.fr/images/stories/PosterExtAbstracts/P_BLS17_Morille.pdf, 2010.

Morille, Y., Haeffelin, M., Drobinski, P. and Pelon, J.: STRAT: An Automated Algorithm to Retrieve the Vertical Structure of the Atmosphere from Single-Channel Lidar Data, J. Atmos. Ocean. Technol., 24(5), 761–775, doi:10.1175/JTECH2008.1, 2007.

Münkel, C., Eresmaa, N., Räsänen, J. and Karppinen, A.: Retrieval of mixing height and dust concentration with lidar ceilometer, Boundary-Layer Meteorol., 124(1), 117–128, doi:10.1007/s10546-006-9103-3, 2007.

Pal, S., Haeffelin, M. and Batchvarova, E.: Exploring a geophysical process-based attribution technique for the determination of the atmospheric boundary layer depth using aerosol lidar and near-surface meteorological measurements, J. Geophys. Res. Atmos., 118(16), 9277–9295, doi:10.1002/jgrd.50710, 2013.

Perona, P. and Malik, J.: Scale-space and edge detection using anisotropic diffusion, IEEE Trans. Pattern Anal. Mach. Intell., 12(7), 629–639, doi:10.1109/34.56205, 1990.

Piironen, A. K. and Eloranta, E. W.: Convective boundary layer mean depths and cloud geometrical properties obtained from volume imaging lidar data, J. Geophys. Res., 100(D12), 25569–25576, doi:10.1029/94JD02604, 1995.

Steyn, D. G., Baldi, M. and Hoff, R. M.: The Detection of Mixed Layer Depth and Entrainment Zone Thickness from Lidar Backscatter Profiles, J. Atmos. Ocean. Technol., 16(7), 953–959, doi:10.1175/1520-0426(1999)016<0953:TDOMLD>2.0.CO;2, 1999.

Stull, R. B.: An Introduction to Boundary Layer Meteorology, edited by R. B. Stull, Springer Netherlands, Dordrecht., 1988.

Szintai, B.: Improving the turbulence coupling between high resolution numerical weather prediction models and Lagrangian particle dispersion models, Swiss Federal Institute of Technology, Lausanne, November., 2010.

Toledo, D., Córdoba-Jabonero, C. and Gil-Ojeda, M.: Cluster Analysis: A New Approach Applied to Lidar Measurements for Atmospheric Boundary Layer Height Estimation, J. Atmos. Ocean. Technol., 31(2), 422–436, doi:10.1175/JTECH-D-12-00253.1, 2014.

Tomás, S., Rocadenbosch, F. and Sicard, M.: Atmospheric boundary-layer height estimation by adaptive Kalman filtering of lidar data, in Proc. of SPIE, vol. 7827, edited by R. H. Picard, K. Schäfer, A. Comeron, and M. van Weele, pp. 782704–782704–10., 2010.

Vuilleumier, L., Hauser, M., Félix, C., Vignola, F., Blanc, P., Kazantzidis, A., and Calpini, B.: Accuracy of ground surface broadband shortwave radiation monitoring, J. Geophys. Res., 119, 13838–13860, doi:10.1002/2014JD022335, 2014.

Wiegner, M. and Geiß, A.: Aerosol profiling with the Jenoptik ceilometer CHM15kx, Atmos. Meas. Tech., 5(8), 1953–1964, doi:10.5194/amt-5-1953-2012, 2012.

Wiegner, M., Madonna, F., Binietoglou, I., Forkel, R., Gasteiger, J., Geiß, A., Pappalardo, G., Schäfer, K. and Thomas, W.: What is the benefit of ceilometers for aerosol remote sensing? An answer from EARLINET, Atmos. Meas. Tech., 7(7), 1979–1997, doi:10.5194/amt-7-1979-2014, 2014

Zellweger, C., J. Forrer, P. Hofer, S. Nyeki, B. Schwarzenbach, E. Weingartner, A. Ammann, and U. Baltensperger: Partitioning of reactive nitrogen (NOy) and dependence on meteorological conditions in the lower free troposphere, Atmos. Chem. Phys., 3, 779-796, 2003.

Zieger, P., Kienast-Sjögren, E., Starace, M., von Bismarck, J., Bukowiecki, N., Baltensperger, U.,

Wienhold, F. G., Peter, T., Ruhtz, T., Collaud Coen, M., Vuilleumier, L., Maier, O., Emili, E., Popp, C., and Weingartner, E.: Spatial variation of aerosol optical properties around the high-alpine site Jungfraujoch (3580 m a.s.l.), Atmos. Chem. Phys., 12, 7231-7249, doi:10.5194/acp-12-7231-2012, 2012

List of Acronyms

Acronym	Description
AL	Aerosol Layer
BL	Boundary Layer
bR	bulk Richardson
CAL	Continuous Aerosol Layer
CBH	Cloud Base Height
CBL	Convective Boundary Layer
CBLH	Convective Boundary Layer Height
EZ	Entrainment Zone
FT	Free Troposphere
JFJ	Jungfraujoch
KSE	Kleine Scheidegg
LCBL	Local Convective Boundary Layer
LCBLH	LCBL Height
LIDAR	Light Detection And Ranging
liminf	Minimum altitude limit
limphys	physically meaningful altitude limit
MAAP	Multi-Angle Absorption Photometer
ML	Mixed Layer
MWR	MicroWave Radiometer
PathfinderTURB	Pathfinder method based on turbulence
PAY	Payerne
PM	Parcel Method
Ri_b	bulk Richardson number
RL	Residual Layer
RS	Radiosonde
SNR	Signal-to-Noise Ratio
TCAL	Top of Continuous Aerosol Layer

Formatted: English (U.S.)